11A

Battelle
Pacific Northwest Laboratories
Richland, Washington 99352

BNWL-1608
Special
Distribution

AEC Research and Development Report

STUDY OF THE REACTIVITY EFFECTS OF FINITE PuO_2 PARTICLE SIZES IN MIXED PuO_2-UO_2 NUCLEAR FUELS

August 1971

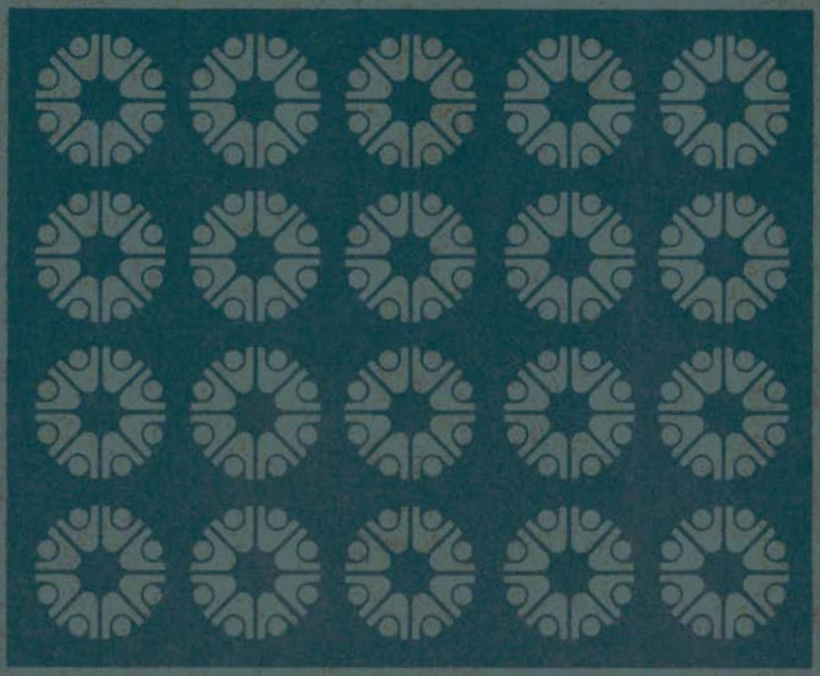

BNWL-1608

PACIFIC NORTHWEST LABORATORY
operated by
BATTELLE
for the
U.S. ATOMIC ENERGY COMMISSION
Under Contract AT(45-1)-1830

BNWL-1608
Special Distribution

STUDY OF THE REACTIVITY EFFECTS OF FINITE PuO_2 PARTICLE SIZES IN MIXED PuO_2-UO_2 NUCLEAR FUELS

by

A. D. Vaughn
Reactor Physics Department

August 1971

BATTELLE
PACIFIC NORTHWEST LABORATORIES
RICHLAND, WASHINGTON 99352

TABLE OF CONTENTS

LIST OF TABLES. v

LIST OF FIGURES viii

ACKNOWLEDGEMENTS. x

INTRODUCTION. 1

SUMMARY 3

DESCRIPTION OF THE LATTICE AND FUEL 4

A. PCTR Test Lattice and Buffer Cells. 4

B. Mixed Oxide Particle Fuel Rods. 8

DESCRIPTION OF THE EXPERIMENT 15

A. Null Reactivity Method. 15

1. Spectrum Matching 16

2. Null Reactivity Measurements. 17

3. Measurement of Cell Worths With Respect to PuO_2 Particles 18

4. Analysis of Null Reactivity Data. . . . 22

5. Cell Worths in Terms of Reactivity. . . 22

B. Reaction Rate and Self-Shielding Measurements 26

1. Copper Foil Irradiations and Flux Traverses 26

2. Separable Foil Holding Fuel Rods. . . . 28

3. Description of the Foils Containing Particulate Fuel 34
4. Description of Other Fission Foils . . . 34
5. Corrections to Foil Data 36
6. Irradiation and Foil Analysis Techniques 42
7. Measured and Calculated Reaction Rates with Respect to Particle Size. 43
8. Calculated Reaction Rates and Self-Shielding Effects. 44
C. Analysis of Enrichment Content by Gamma Scanning 47
1. Chemistry Analysis 50
2. Gamma Scanning 50
3. Conclusions Derived From Scanning Measurements. 62
D. Neutron Cross Section Generating Techniques and Other Group Constants. 64
1. Theoretical Calculation Methods and Programs 66
E. Determination of k_{∞}^{*} From The Null Reactivity Experimental Data. 67

1. Theory Definition of k_∞^* In The Poisoned Lattice Technique. 67

2. Results (k* by Null Reactivity Technique). 73

3. Normalization of Measured k_∞^* to Equivalent Fuel Density. 73

F. Determination of k* From The Adjoint Weighted Cross Section Technique (Unpoisoned Technique) 76

1. Theory-Definition of k_∞^* From the Unpoisoned Technique 76

2. Measured k_∞^* From Adjoint Weighted Cross Section Data 78

G. Comparison of Theory and Experiment. 80

1. Definition of Theoretical k_∞' 80

2. Derivation of Mis-Match Corrections for Unpoisoned Technique 82

3. Determination of Measured k_∞' In The Fundamental Mode 83

4. Theoretical Quantities of k_∞' for Water and Graphite Lattices. 83

H. Conclusions Concerning Particle Effects From This Study 86

REFERENCES 89

APPENDIX A 92

APPENDIX B 94

APPENDIX C 100

LIST OF TABLES

Table I. List of Mixed-Oxide Particulate Fuel Rods and Respective Reactivity Worths in Center of PCTR Test Cavity 10

Table II. Summary of Reactivity Data Derived by Null Reactivity Technique With Poisoned Lattice Cells 23

Table III. Test Cell Worths in Terms of Mass of Copper (M_o). 24

Table IV. Relative Activities and Radial Location of Copper Foils Irradiated in Center Test Cell. 29

Table V. Results From Chemical Analysis of Pu-Al Foil #3 39

Table VI. Relative Plutonium Foil Activities With Respect to PuO_2 Particle Size 45

Table VII. Relative ^{235}U Foil Activities With Respect to PuO_2 Particle Size 45

Table VIII. Relative Copper Foil Activities With Respect to PuO_2 Particle Size 45

Table IX. Results From Analysis of UO_2-PuO_2 Fuel Rod Specimens. 51

Table X. Average Integrated Counts From Specific Photo Peaks With Respect to Mixed Oxide Particle Rod Sets. 58

Table XI. Attenuation Factors and Correction to Integrated Photo Peaks 60

Table XII. Enrichment of PuO_2-UO_2 Particle Fuel Determined by Gamma Scanning, Chemistry and Reactivity Measurements... 63

Table XIII. Corrected Isotopic Densities of Particle Fuel Rods. 65

Table XIV. Measured Relative Production and Absorption Terms for the Derivation of k* by the Null Reactivity Method. 74

Table XV. Measured and Calculated Quantities to Determine k* by Unpoisoned Method 79

Table XVI. List of Corrections to Determine k_∞' for Comparison to the Fundamental Model Calculation. 84

Table XVII. Calculated k' for Graphite and Water Moderated Lattice With Respect to Particle Size 85

Table VIII. Summary of Experimental and Theoretical Parameters of Particle Fuel 87

LIST OF FIGURES

Figure 1. PCTR Test Cavity With 4" Graphite Lattice and 2% PuO_2-UO_2 Particulate Fuel Rods. . . . 6

Figure 2. PCTR Test Lattice Showing Removal of the Four Central Lattice Cells for Cell Worth Measurements. 7

Figure 3. Fuel Arrangement in and Around the PCTR Test Cavity 9

Figure 4. Auto-Radiograph of Solid Solution Fuel Pellet 12

Figure 5. Auto-Radiograph of Pellet Containing 350 Micron PuO_2 Particles. 13

Figure 6. Illustration of Fuel Changing Via Rear Face Port in PCTR 19

Figure 7. Diagram of Copper Foils and Pins in Center Cell 27

Figure 8. Measured vs. Calculated Relative Reaction Rates of Copper Foils in Center Test Cells. 30

Figure 9. Axial Flux Traverse From Relative Copper Foil Measurements Along Center Test Cell . .31

Figure 10. Graphite Foil Holders and Separable Fuel Rods 33

Figure 11. Diagram of Particle Foils Containing PuO_2 Particles. 35

Figure 12. Diagram of Al-Pu Foils Containing A Homogeneous Mixture of Pu and Aluminum. . 35

Figure 13. Comparison of Calculated and Measured Self-Shielding Effects in Plutonium With Respect to Particle Size. 48

Figure 14. Comparison of Calculated and Measured Self-Shielding Effects in Uranium With Respect to Particle Size. 49

Figure 15. Ge-Li Detector System to Determine Enrichment in Mixed Oxide Fuel Rods 53

Figure 16. Graphic Presentation of Photo Peaks Measured During Scanning of Mixed Oxide Fuel Rods 8BMB. 56

ACKNOWLEDGEMENTS

I wish to acknowledge the direction and suggestions offered to me during this project by Dr. Maurice A. Robkin of the University of Washington and Dr. David D. Lanning, formerly of Battelle-Northwest and now at Massachusetts Institute of Technology and Dr. Loren C. Schmid of Battelle-Northwest, who served as my advisor at Battelle-Northwest after Dr. Lanning's transfer to Massachusetts. The technicians who handled the foil counting tasks; namely, Mr. I. N. Sorrells, Jr. and Mr. J. E. Choate, are to be commended for the long tedious hours they spent in the foil counting laboratory. Mr. Clifford Richey offered considerable direction during the theoretical calculations and also provided training with the computer codes involved in this work. Last, but not the least, I am grateful to Betty Compton for typing this manuscript.

A STUDY OF THE NEUTRONIC EFFECTS OF PuO_2 PARTICLES ON REACTIVITY

Arlie Dwayne Vaughn

INTRODUCTION

Fuel development for plutonium recycle has led to fuels composed of the mixed oxides of plutonium and uranium. The fabrication process presently used in manufacturing of plutonium fuels result in the plutonium being distributed throughout the uranium as particles. Power generation of these fuels occurs mainly in the plutonium particles mixed into the UO_2. Due to self-shielding properties of the particles, the reactivity of the fuel is dependent on particle size[1]. Experimental and theoretical information about particle size on the characteristics of the reactor system is thus important for determining its impact on safety and economics.

The reactivity effect of changing the PuO_2 particle size is complex due to the interaction of ^{239}Pu fission and absorption combined with the ^{240}Pu absorption. Shielding of the ^{239}Pu with increasing particle size reduces the absorption probability, but due to the shielding of the low lying resonance of ^{239}Pu capture-to-fission ratio α decreases with increasing particle size. In addition, the shielding of the ^{240}Pu resonance is important and its positive reactivity effect

with increasing particle size depends on the ^{240}Pu concentration. The combination of these positive and negative effects can give net reactivity effects in either direction depending on the concentration and particle size involved.

Although there have been experiments and calculations made in the area of particle size effect studies[2,3], there has not been a conclusive set of experiments complete and analyzed for PuO_2 particle size reactivity effects.

Therefore, the infinite medium neutron multiplication factors of separate UO_2-2% PuO_2 (8% ^{240}Pu) fuel rods containing plutonium oxide ranging between a solid solution state to particle sizes of 330 microns respectively have been measured in the PCTR. Due to the non-homogeneity of the experimental fuel rods, a special set of aluminum foils containing plutonium oxide particles were utilized to obtain the relative neutron production and absorption rates in the experimental fuel assemblies.

The reactivity worths of the mixed oxide rods, measured in the PCTR, and the relative absorption rates determined from the foil data indicated the fuel rods were not uniformly enriched. Therefore, the rods were analyzed for enrichment content by gamma scanning measurements which were normalized to chemistry samples to derive corrected plutonium content in each test rod.

A number of theoretical calculations were performed in conjunction with the experimental measurements to aid in the analysis and interpretation of the experimental results. These calculations were repeated for water and graphite lattices other than the experimental model to derive the particle effects that can be expected in different reactor types. A discussion of the theoretical results is presented.

SUMMARY

The neutronic parameters of 2 wt% (8% ^{240}Pu) particles in naturally enriched UO_2 diluent were determined using the null reactivity technique and the adjoint weighted cross section technique in the Physical Constant Testing Reactor (PCTR) at room temperature. The measurements and subsequent analysis indicate:

1. The reactivity effects of the mixed oxide rods decrease with increasing particle size. The mass of copper required to maintain unit neutron multiplication in the PCTR decreased by 20 percent when the PuO_2 particle size increased from 50 to 330 microns.
2. The cell worths in terms of direct reactivity changes due to replacement of fuel of a smaller particle size in the center test cell by fuel with a larger particle size showed similar decrease in reactivity worths.

3. The measured neutron reaction rates of the elements in the fuel mixture verify that the fissionable isotopes in the larger particles are more self-shielded than in particles of smaller diameter. These measured self-shielding effects were in excellent agreement with the calculation of these same effects.

4. The infinite medium neutron multiplication factors derived by the PCTR measurements indicate trends of decreasing reactivity with respect to particle size which are similar to two group calculations of these same effects. The large k_∞ ~(1.500) which was measured for the system produced statistical uncertainties (10 mk) larger than the reactivity differences estimated to result from the reactivity effect due to particle size. However, the relative uncertainties between measurements are expected to be less than 5.0 mk and do indicate the changes in the reactivity.

DESCRIPTION OF THE LATTICE AND FUEL

A. PCTR Test Lattice and Buffer Cells

The null reactivity technique[4] and the adjoint-weighted cross section technique[5] were used for determining k_∞[6] for 0.5-inch diameter UO_2 rods in which PuO_2 particles are embedded. These fuel assemblies were arrayed inside the PCTR

test cavity which is 41.25 inches x 41.25 inches x 37.5 inches.

The test cells in the PCTR cavity were 4.0-inch square graphite blocks 37.5 inches long. The blocks were undercut 0.030 inches deep and three-inches wide along the axial face so that strips of copper could be inserted between the cells during the null reactivity measurements.

The graphite blocks were drilled to contain the fuel rods. These fuel channels were 0.69 inches I.D. and extend the length of each block.

The complete test lattice in the PCTR cavity consisted of an eight by eight array of the four inch graphite blocks. This arrangement is depicted in Figure 1, with the PCTR driver pattern during the null reactivity measurements with copper strips between the cells.

The four cells in the center of the test lattice were divided into three longitudinal sections, 8.75 inches, 20.0 inches, and 8.75 inches, respectively. The two shorter elements are termed front and rear buffer cells and the longer element is usually referred to as the center cell.

The twenty-inch center cells provide the strategic locations for deriving the experimental data from the test lattice. All the lattices around the four center cells are also called buffer cells. Figure 2 shows the four center cells being removed from the PCTR test cavity.

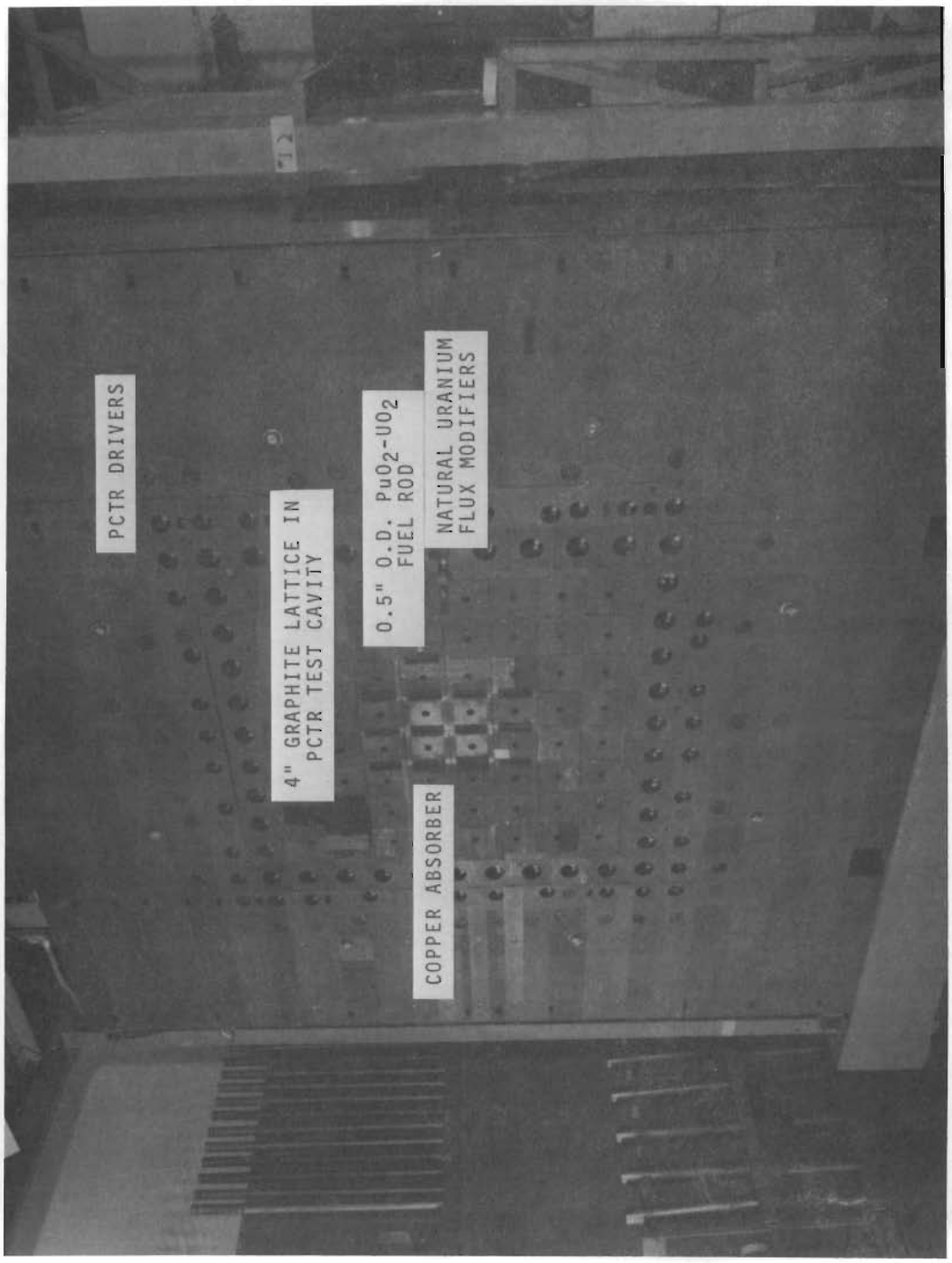

Figure 1. PCTR Test Cavity with 4" Graphite Lattice and PuO_2-UO_2 Fuel Rods

Figure 2. PCTR Test Lattice Showing Removal of the Four Central Lattice Cells for Cell Worth Measurements

The four center cells of the array contained rods of either the solid solution set or a specific particle set, depending on the measurement. Sixty cells surrounding the four center cells contained UO_2-2 wt% PuO_2 homogeneous fuel (Figure 3). The reactor was made critical by the addition of PCTR drivers around the test cavity; the drivers are one inch O.D. rods containing $^{235}UO_2$ in lead.

B. Mixed Oxide Particle Fuel Rods

The development of a process to make a uniform particle fuel of adequate specifications to satisfy the criteria for the experiment began in early 1965[7], and the rods were completed approximately one and one-half years later with various alterations to the manufacturing methods as the technology improved.

A complete list of the various rod sets which were manufactured for the PCTR experiment is presented in Table I. The list includes ten separate rod sets (four rods per set), 20 inches long, clad in zirconium tubing 0.030 inches thick and with 0.565-in.O.D. Originally, five rod sets were required with distinct fuel geometries including a solid solution or homogeneous mixture of UO_2 and PuO_2, or one of four PuO_2 particle sizes ranging from 50 microns to 330 microns. Additional sets of rods with similar particle sizes were made as the particle manufacturing techniques were developed.

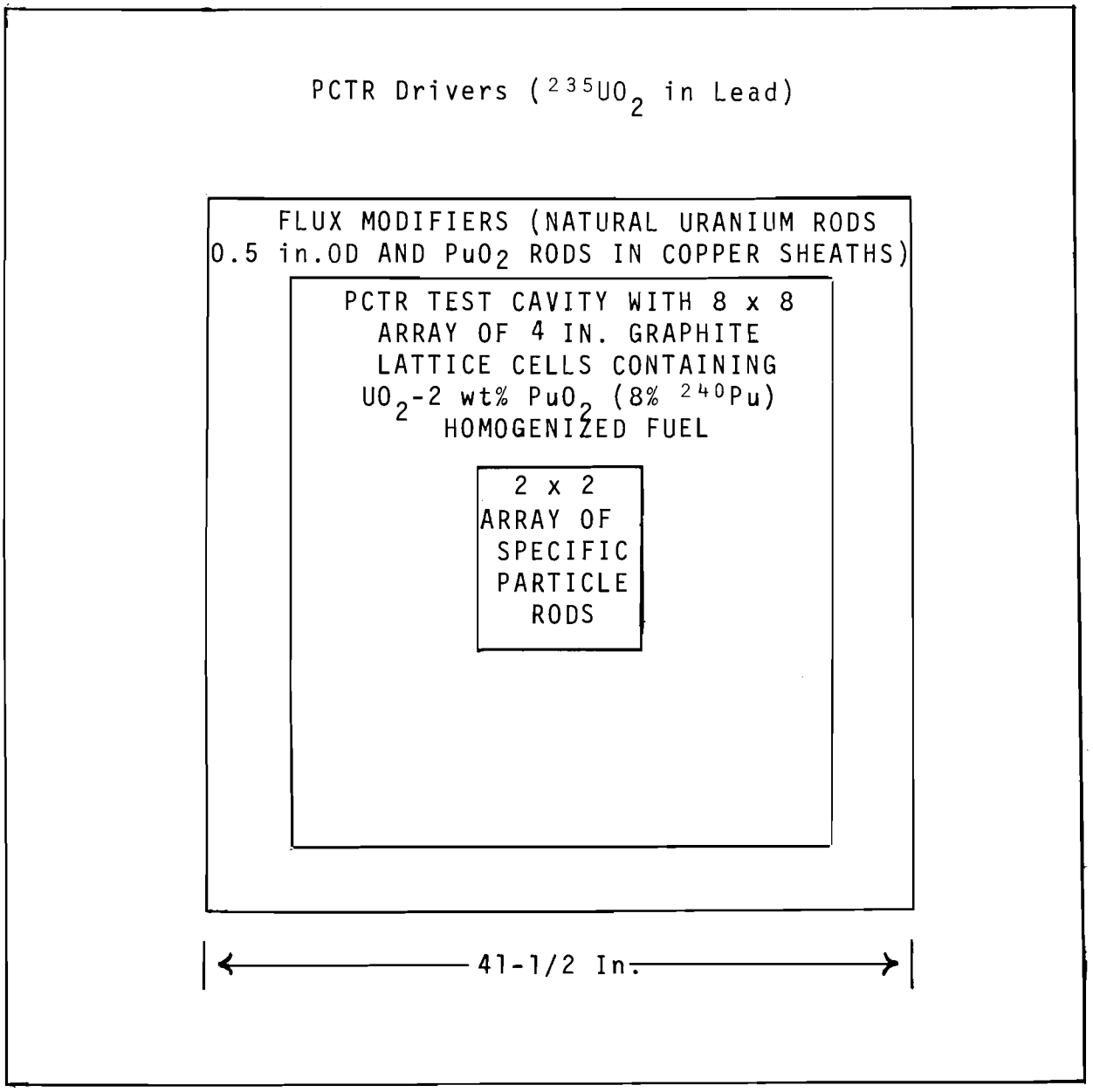

(NOT DRAWN TO SCALE)

Figure 3. Fuel Arrangement In and Around PCTR Test Cavity

Table I. List of Mixed-Oxide Particulate Fuel Rods and Respective Reactivity Worths In Center of PCTR Test Cavity

Rod Designator	# Rods In Set	Rod Type	Density g/cc	Mass of Cu. for Unit k grams	Reactivity Worth ¢
8SC	4	Solid solution Ball milled (Mfg from same material as 8RA350)	8.704	455.22 ±3.58	37.76 ± .33
8BMB	4	Solid solution Ball milled (Mfg from same material as 8B rods)	8.571	474.73 ±2.08	38.19 ± .32
8BME	1	Solid solution Ball milled (last rod manufactured)	8.474	463.50 ±2.54	38.12 ± .34
8P50	4	50 Micron Induction plasma	8.601	495.39 ±2.39	39.12 ± .33
8B100	4	110 Micron Jet milled	8.739	501.57 ±2.35	39.29 ± .33
8P100	4	110 Micron Induction plasma	8.638	489.08 ±2.53	39.01 ± .33
8B200	4	200 Micron Jet milled	8.718	471.80 ±2.99	38.28 ± .33
8P200	4	200 Micron Induction plasma	8.657	468.75 ±3.28	38.31 ± .33
8RA350	2	330 Micron Jet milled (Vibration tested for roundness)	8.798	446.75 ±3.88	37.37 ± .33
8B350	4	330 Micron Jet milled	8.691	453.89 ±4.56	37.82 ± .33

All the solid solution rods were manufactured by ball milling the material before mixing. The particle fuel was initially made by jet milling the oxides before mixing and then testing the pellets for roundness by a vibrational test on an incline plane which would separate the round pellets from those which were not round. Rod set 8RA350 were the only rods made with the initial process method because the vibration test eliminated too many of the particles. The jet milling process was continued for rod sets 8B100, 8B200 and 8B350 using a screening method to obtain spherical particles. A third method[8] was developed which consisted of dropping granular material through an induction heated plasma. The particle rod sets manufactured in the induction plasma method have been designated 8P50, 8P100 and 8P200.

To insure that the plutonium was distributed evenly through the fuel rods, samples of the same fuel material were polished and then given an alpha-auto-radiograph. These graphs are depicted in Figures 4 and 5 and indicate no discrepancies in the homogeneity of the UO_2 and PuO_2 mixture. However, it will be shown later that the measured reactivity variations in the rods were not in agreement with the changes in the measured neutron absorption rates with respect to particle size. Further investigation proved that some of the rods were over-enriched as much as twenty percent and there-

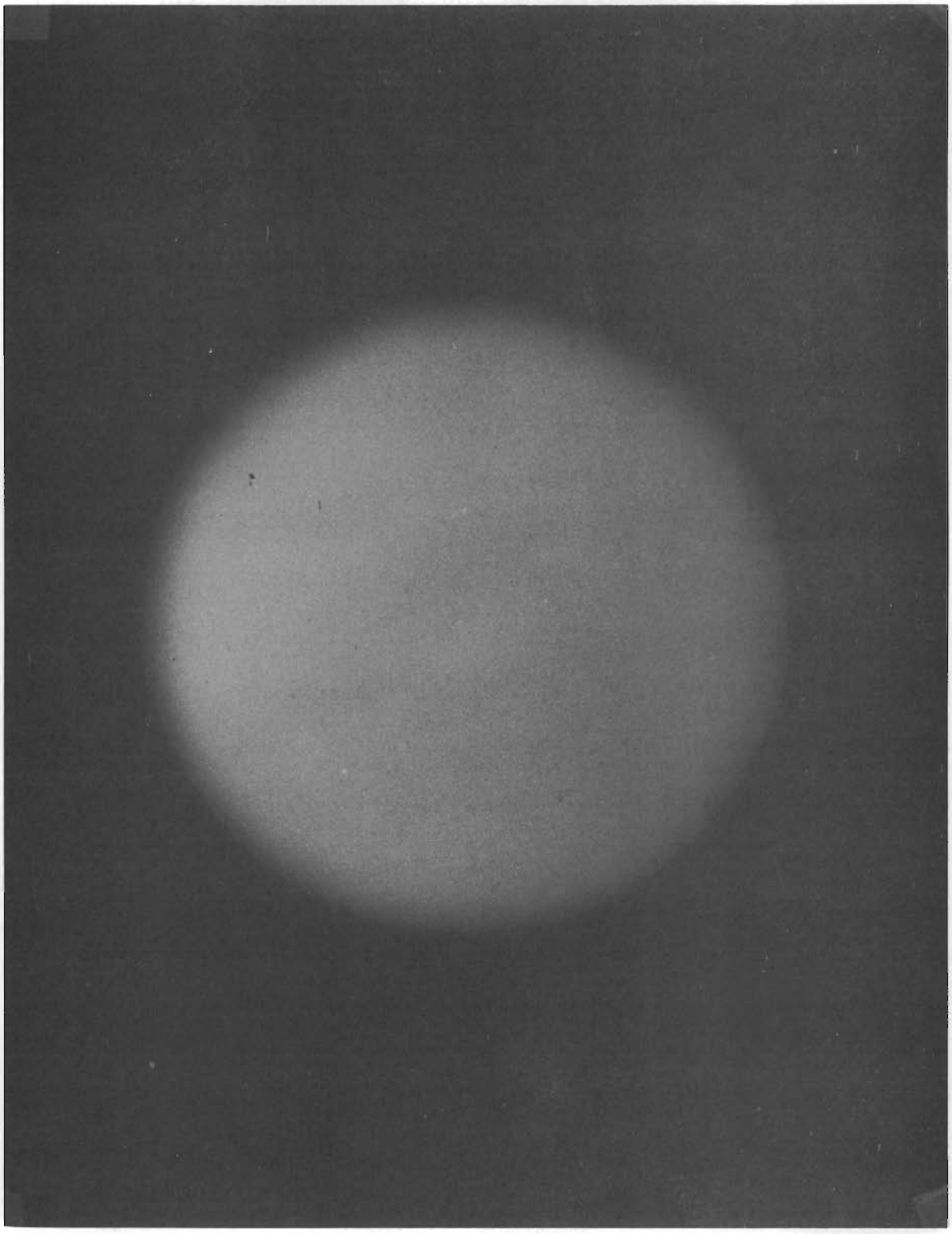

Figure 4. Autoradiograph of Solid Solution Fuel Pellet

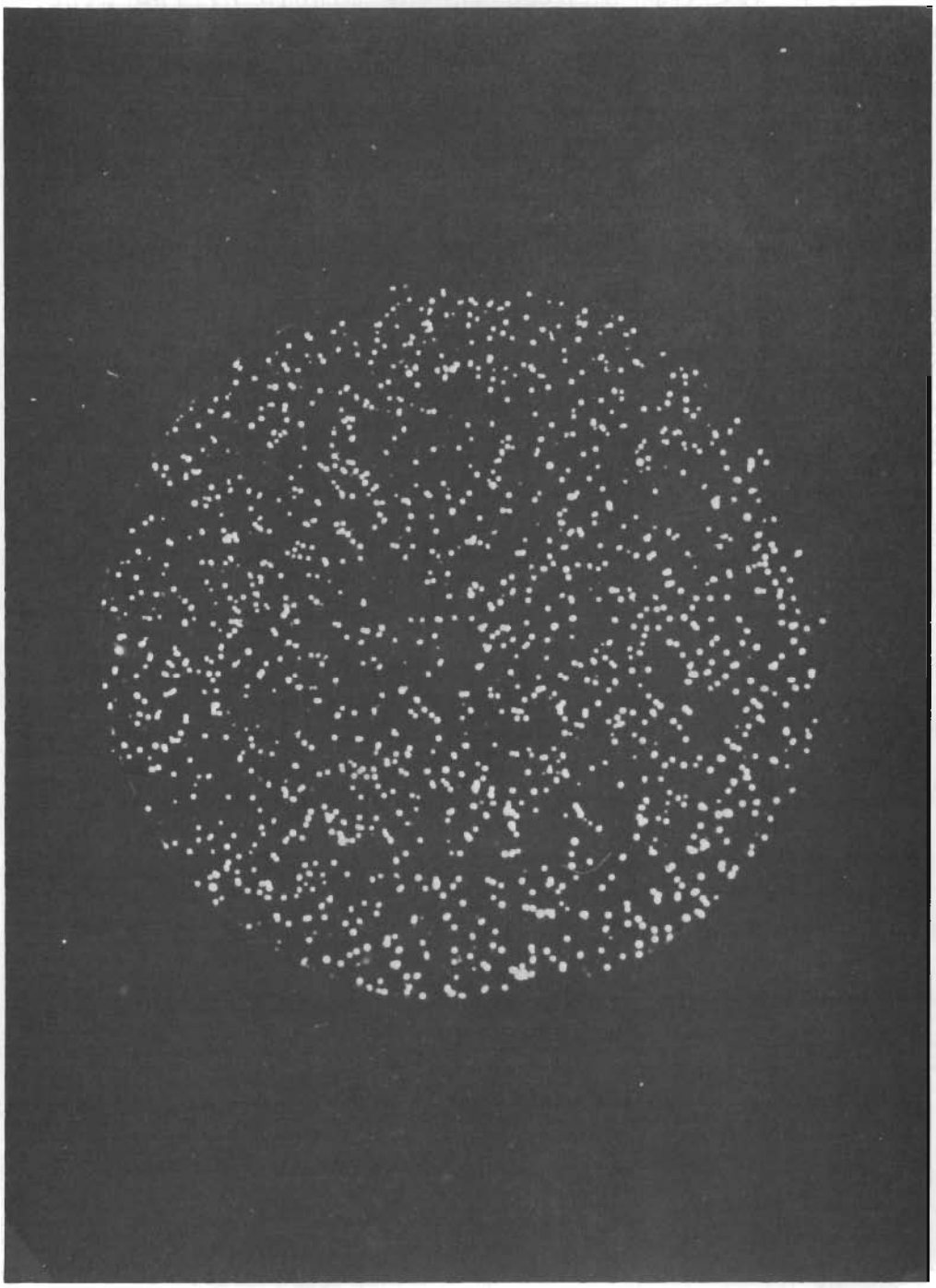

Figure 5. Autoradiograph of Mixed Oxide Pellet Containing 50 Micron Pu-O_2 Particles

fore no enrichment contents are mentioned at this time. A research plan was implemented in the middle of the experiment to determine the amount of plutonium in each rod set by a combination of reactivity data, a few chemistry samples, and an extensive measurement of the gamma-ray photo-peaks emitted from plutonium isotopes. This technique and the analysis will be discussed in a later section.

The exact particle specifications were not able to be maintained so that the average size of the particles passing through the sizing screen results in a sphere slightly different than the nominal size listed in the rod designator. The average particle size in the specific rod sets were determined by measuring the weight of a counted number of particles, using the theoretical density of PuO_2 at 11.47 g/cc, and calculating the average spherical volume and diameter. The measured factors and results are as follows:

Nominal Particle Size	No. of Particles Weighed	Weight (g)		Effective Particle Radius
50	None	Extrapolated data	=	51 microns
100	150	.0011	=	110 microns
200	88	.0039	=	200 microns
350	45	.0095	=	330 microns

The densities of the rods were derived from the manufacturing data which was primarily a gross measurement of the

fuel in the rod. An empty clad piece was measured to derive the volume of each rod and the densities were calculated. It is not certain that the fuel is stochiometric nor is it possible to put errors on the density parameters which definitely affect the isotopic concentrations of the fuel.

DESCRIPTION OF THE EXPERIMENT

The method for determining the neutron multiplication factors for test lattices in the Physical Constants Testing Reactor (PCTR) can be done by two different techniques called the null reactivity method and the adjoint weighted cross section method. Some of the measurements and data acquired with the PCTR are applicable to both methods of analysis.

A. Null Reactivity Method

Basically, the PCTR experiment using the null reactivity method follows these procedures:

- Spectrum matching, which is the adjustment of the neutron energy spectrum so that it is identical with the spectrum present in an infinite array of test cells.
- Neutron absorber measurements to determine the amount of neutron absorber (copper) required to achieve unit multiplication in the test cell.

- Measurement of the relative reaction rates of the components of the test cell in both the lattice reduced to unit multiplication with copper and the lattice without the copper.

1. Spectrum Matching

The thermal to epi-thermal neutron flux ratios were inferred by measuring cadmium ratios of 0.005-inch thick gold foils and comparing the cadmium ratio in the center test cell with the values obtained at an equivalent location in a buffer region. The gold, when covered with cadmium, is activated almost entirely by neutrons in a narrow energy region around 4.9 ev. The large number of foils necessary for this measurement usually have slightly different thicknesses and therefore the cadmium ratios must be corrected to a standard foil thickness using experimental data published by R. A. Bennett[9].

For this particular experiment the lattice pitch was sufficiently small that an eight by eight array of test cells could be inserted into the PCTR test cavity. With this large array of buffer cells similar to the center test cell, it was possible to obtain a constant gold cadmium ratio throughout the center region. A constant gold cadmium ratio in the two energy group approximation

implies a constant neutron spectrum.

It must be noted that the spectrum matching was accomplished with 2 wt% enriched homogeneous mixed oxide fuel in the buffer cells and 2 wt% enriched solid solution rods in the center cells. No cadmium ratio measurements were attempted with the particulate fuel rods in the center cells. Spectrum mis-match corrections had to be calculated to interpret the measured data for the particulate fuel due to enrichment differences between the center cell and radial buffer fuel. These calculations are described in Section G, paragraph 2 of this report.

2. Null Reactivity Measurements

The null reactivity technique depends on the observation that a properly poisoned cell will have the same reactivity effect on the reactor as will an empty cavity. In a properly poisoned cell the neutron absorptions balance the productions. The central test cell was shown being removed in Figure 2 (page 7). Short end buffer cells enclose the central cell along the long axis. Slots are provided in the lattice for the insertion of the copper poison strips at the cell boundaries.

A reactivity series was completed for each loading for which the cadmium ratio of gold was measured. The

basic technique to determine the mass of copper (M_o) necessary for unit multiplication has been simplified to the equation below:

$$M_o = \frac{\rho \text{ cell in} - \rho \text{ cell out}}{\text{Units of reactivity per gram of Absorber}} + M_{\text{copper}}^{\text{boundary}}$$

Where $M_{\text{copper}}^{\text{boundary}}$ = Mass of copper on the cell boundaries;

ρ cell in = PCTR reactivity with cell in;

ρ cell out= PCTR reactivity with cell out, corrected to exclude nitrogen effects.

3. Measurement of Cell Worths With Respect to Particle Size

For large center cells which exceed the size of the opening into the movable face of the PCTR it is necessary to open the face for cell changes. The standard deviation for reactivity measurements were reduced from $\pm 0.04¢$ to $\pm .02¢$ by devising a system by which the movable face could remain closed and changes to the center cells could be made via a port in the rear face. Figure 6 illustrates the methods for changing fuel rods via the rear face port by first removing 1-inch O.D. graphite dowels from the front buffer region of the movable face which provided openings to the fuel channels containing the four center cell rods. The 8.75-inch front buffer rods were removed first and then the center cell fuel rods could be withdrawn and

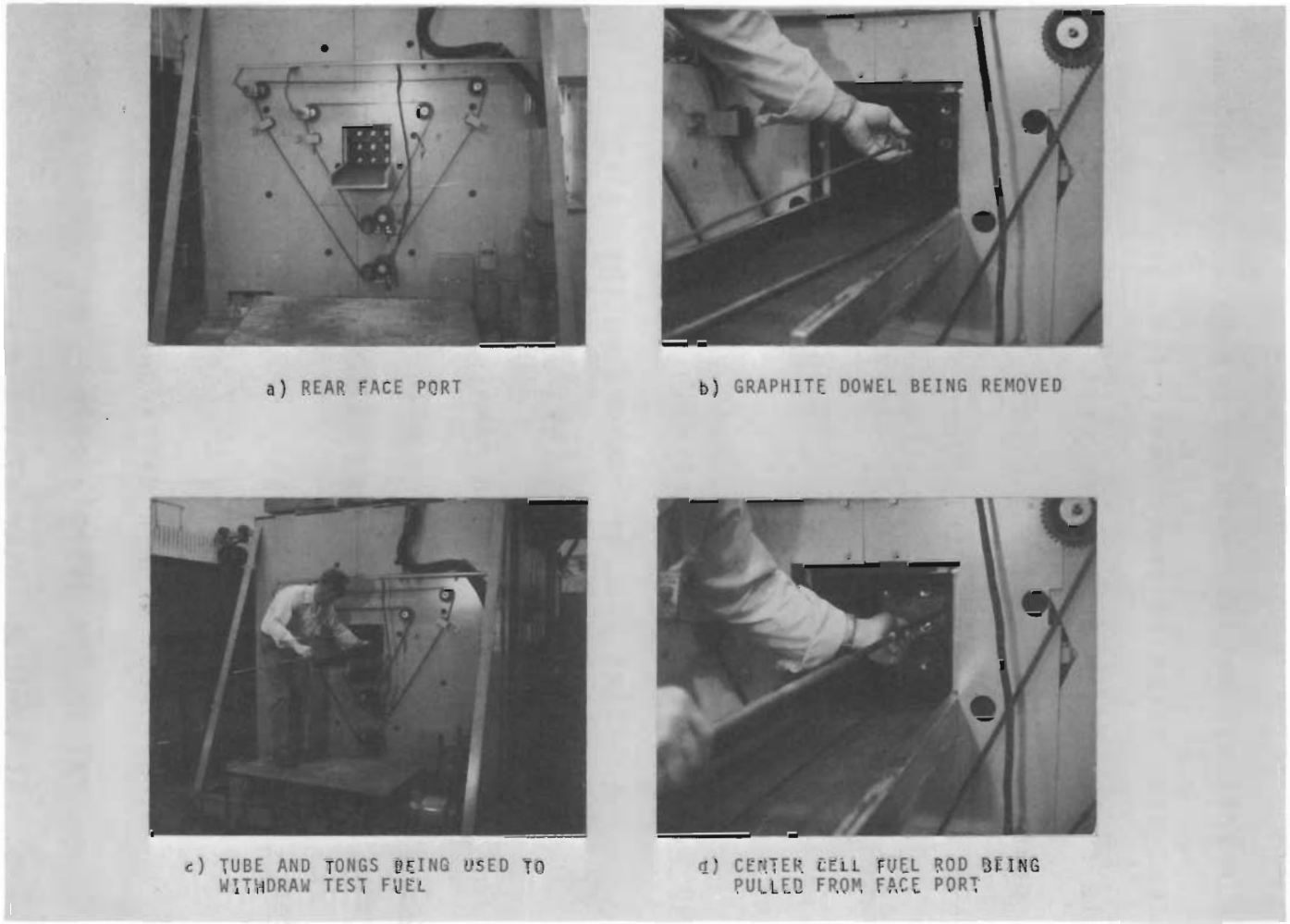

Figure 6. Illustration of Fuel Changing Procedure via Rear Face Port in PCTR

exchanged. Reactivity measurements could be reproduced to within 0.02¢ by leaving the movable face in position between cell changes.

The reactivity measurements in the matched spectrum conditions were taken at least twice for each set of particle fuel rods in the center test cells. The experimental procedures were quite long due to the number of rods involved and followed this general pattern.

Step 1. Cell in (base case) measurement with rod set 8SC in the four 20-inch center cell locations.

Step 2. Cell in measurement with 8BME solid solution rods by exchanging the rods through channels in the movable face port with the face remaining closed.

Step 3. Cell in measurement with 8BME solid solution rods.

Step 4, etc. The measurements continued, each time by exchanging the four center cell rods with a different particle set in the movable face.

Step 5. At various intervals, rod sets 8SC, solid solution rods, were replaced into the center cells of the reactor to ascertain any reactivity drifts

due to some unknown conditions.

Step 6. When the various particle rods had been measured in the center cell locations, and the base case had been remeasured, the four center cell blocks were removed to make the cell out reactivity measurement. This exchange was also accomplished via the movable face port with the face closed.

Step 7. The complete series of reactivity measurements, described in Steps 1 through 6, were repeated in order to improve the statistical certainty of each measurement.

Step 8. The reactivity series measurements require the determination of the cell worth in terms of the mass of copper necessary to achieve unit multiplication. Therefore, a copper vs. reactivity standard measurement was made by placing a specific mass of copper at the center cell boundary and measuring the reactivity change.

Step 9. It is necessary to subtract the effects of nitrogen in the cell cavity when the

cell is removed. The reactivity effect of the nitrogen was determined in relation to the reactivity effect of a specific amount of copper in the cell cavity. This method is described in Appendix A.

4. Analysis of Null Reactivity Data

To determine the neutron multiplication factor using the null reactivity technique, it is necessary to determine the worth of the test lattice in terms of a specific amount of copper, as stated previously. The reactivity measurements and respective nitrogen corrections for the null reactivity technique are listed in Table II.

The reactivity worths of the various particle fuel rods are tabulated in terms of the mass of copper (M_o) necessary to achieve unit neutron multiplication in Table III.

5. Cell Worths in Terms of Reactivity

The second experimental method in which the adjoint neutron weighted cross section of the cell is determined includes no copper around the cells for measuring cell worths. Fundamentally the following procedure is followed:

a. A reactivity measurement is made with all cells in place and no extraneous absorbers are in or around the cells.

Table II. Summary of Reactivity Data Derived by Null Reactivity Technique With Poisoned Lattice Cells

Rod Designator	Reactivity Cell in ¢	Reactivity Cell Out ¢	Reactivity Nitrogen ¢	Cell Reactivity* ¢
8SC	20.229 ±0.016	22.702 ±0.028	0.887 ±0.036	-3.360 ±0.048
Solid Solution	20.086 ±0.016	22.597 ±0.040	0.864 ±0.038	-3.375 ±0.057
	20.638 ±0.028	23.095 ±0.040	0.836 ±0.037	-3.294 ±0.061
8BMB	18.757 ±0.040	22.703 ±0.028	0.887 ±0.036	-4.833 ±0.061
Solid Solution	18.605 ±0.040	22.597 ±0.040	0.864 ±0.038	-4.856 ±0.068
8BME	20.099 ±0.040	22.702 ±0.028	0.887 ±0.036	-3.490 ±0.061
Solid Solution	19.883 ±0.040	22.597 ±0.028	0.864 ±0.038	-3.578 ±0.068
	20.435 ±0.040	23.095 ±0.040	0.836 ±0.037	-3.496 ±0.063
8P50	21.916 ±0.040	22.703 ±0.028	0.887 ±0.037	-1.673 ±0.061
50 Micron	21.773 ±0.028	22.597 ±0.040	0.864 ±0.038	-1.689 ±0.068
8B100	22.462 ±0.040	22.703 ±0.028	0.887 ±0.037	-1.128 ±0.061
110 Micron	22.318 ±0.040	22.597 ±0.040	0.864 ±0.050	-1.143 ±0.068
8P100	21.414 ±0.040	22.748 ±0.028	0.887 ±0.037	-2.220 ±0.061
110 Micron	21.271 ±0.028	22.597 ±0.040	0.864 ±0.038	-2.191 ±0.068
8B200	20.036 ±0.040	22.703 ±0.028	0.887 ±0.036	-3.554 ±0.061
200 Micron	19.892 ±0.040	22.597 ±0.040	0.864 ±0.038	-3.569 ±0.068
8P200	19.758 ±0.040	22.703 ±0.028	0.887 ±0.036	-3.832 ±0.061
200 Micron	19.614 ±0.040	22.597 ±0.040	0.836 ±0.037	-3.819 ±0.068
8B350	17.777 ±0.040	22.703 ±0.028	0.887 ±0.036	-5.813 ±0.061
330 Micron	17.633 ±0.040	22.597 ±0.040	0.864 ±0.037	-5.828 ±0.068
8RA350	19.443 ±0.040	22.703 ±0.028	0.887 ±0.036	-4.146 ±0.061
330 Micron				

*Four cells contained 2063.125 grams of copper on their boundaries during these measurements.

Table III. Test Cell Worths in Terms of Mass of Copper (M_o)

Rod Type	M_o (grams) Four Cell	One Cell
8SC - Solid Solution (four rods)	1898.60 1896.93	474.73 ± 2.08
8BMB - Solid Solution (four rods)	1820.52 1821.27	455.22 ± 3.60
8BME - Solid Solution (one rod with 3 of rod set 8SC)	1887.74 1886.42 1888.93	*463.50 ± 2.54
8P50 - 50 Micron (four rods)	1982.37 1980.72	495.39 ± 2.39
8B100 - 110 Micron (four rods)	2007.04 2005.55	501.57 ± 3.33
8P100 - 110 Micron (four rods)	1956.23 1956.41	489.08 ± 2.53
8B200 - 200 Micron (four rods)	1888.66 1885.72	471.80 ± 2.99
8P200 - 200 Micron (four rods)	1876.48	468.75 ± 3.28
8B350 - 330 Micron	1790.35 1783.72	446.76 ± 3.88
8RA350 - 330 Micron (two rods with two of rod set 8SC SS Rods)	1857.27	*453.90 ± 5.01
8BME - Solid Solution (one rod with three of rod set 8BMB SS Rods)	1830.97 1834.22	*466.12 ± 3.30

*These values have been interpolated so that they apply to the one or two rods with a specific particle size.

b. The center cells are removed and the rods are repositioned to the same position as they were in the first measurement and the reactivity worth of the cell is derived from the increase or decrease in the period.

The process to measure the reactivity worth of the rods was fundamentally the same as in the measurements with copper. Several rod calibration steps were interspaced between sections of cell measurements in order to determine the full worth of all four cells when removed from the reactor because each cell was worth approximately 40¢ and the reactor measurements were limited to periods greater than 20 seconds (≈25¢ reactivity).

The cell worths in terms of the direct reactivity measurements have been included in Table I and corroborate the measured data from the null reactivity technique which are in terms of the mass of copper. As it turned out, the reactivity data and the measured reaction rates were in disagreement with what was theoretically expected for particle self-shielding and therefore the independent sets of reactivity data were assurance that the reactivity measurements techniques were not in error.

B. Reaction Rate and Self-Shielding Measurements

The relative reaction rates of the test cell components are determined from foil activation measurements. The energy dependence of the reaction rates are determined from cadmium ratios.

1. Copper Foil Irradiations and Flux Traverses

After the gold cadmium ratio information has indicated that the test cells have the proper energy distribution, copper foils (0.005-inch thick and 0.5-inch O.D.) and pins (0.036-inch O.D. 0.25-inch long) were strategically placed in the graphite and the fuel. Bare and cadmium covered foils and pins were activated in separate irradiations and the normalization between irradiations were accomplished by placing monitor foils in an external thermal column[10].

The foil locations illustrated in Figure 7 are sufficiently provided so that plots of relative reaction rates across the cell can be made.

Similar foils were placed along the axis of the fuel rod (on the surface of the cladding) and between the cell boundaries to derive axial traverse data.

Copper foils (0.005-inch thickness) were used for traverses in the graphite, in the fuel, and in the air

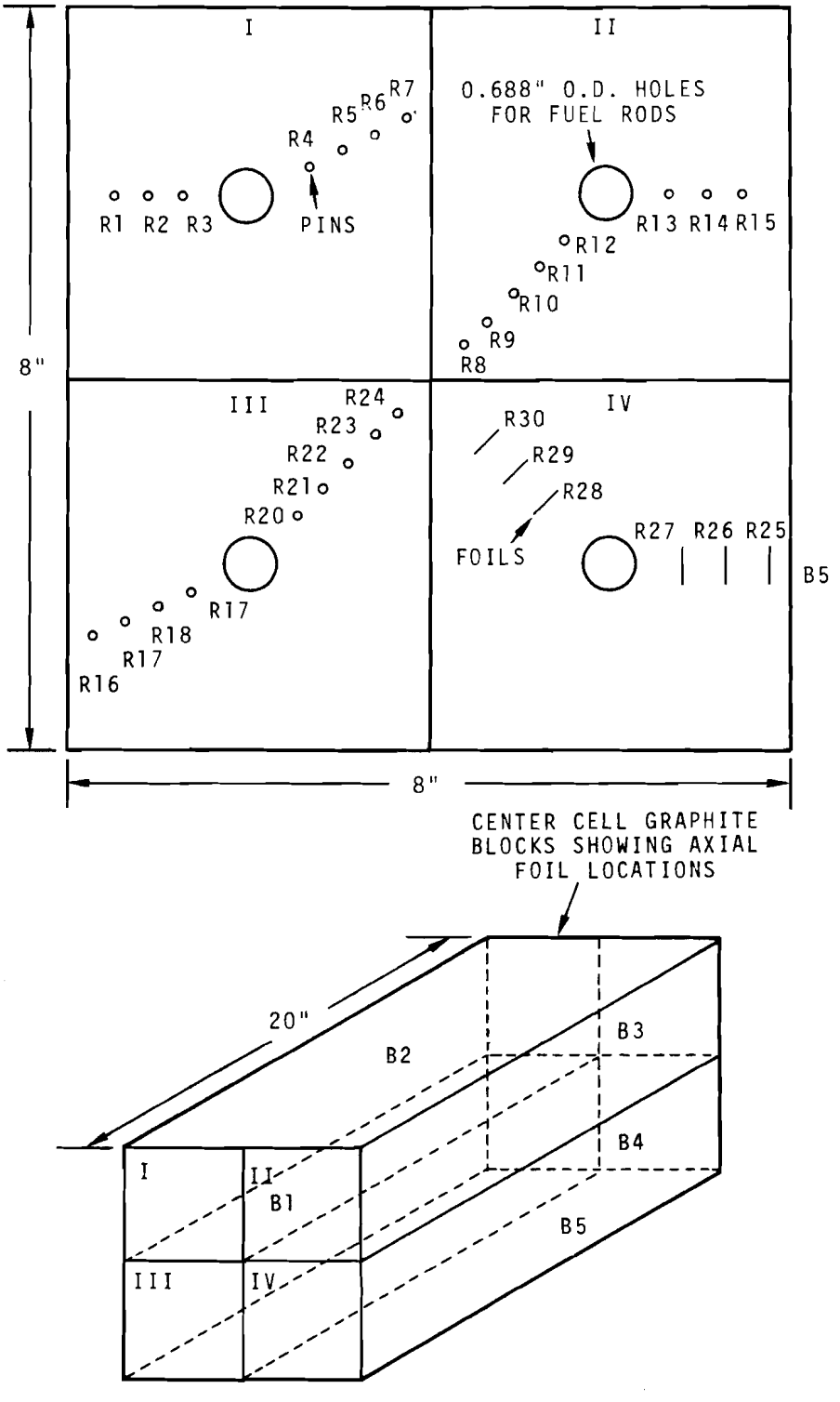

Figure 7. Diagram of Foil and Pin Locations for Radial and Axial Traverses in Center Cells

space between the fuel and the graphite. The specific activities of the copper foils placed in the graphite and other cell regions relative to foil in the external thermal column are presented in Table IV. The activities were calculated using a revised version of the computer code APDAC-I[11], which corrects the counting data for activity decay during counting, room background, foil mass variations, and residual activity.

The spatial variations of the sub-cadmium and epi-cadmium relative copper-64 activities along radial traverse locations are shown in Figure 8 and the axial traverse data is illustrated in Figure 9.

Similar data was measured for the cells with the 330 micron particle rods; however, the pin data was not sufficiently accurate to determine the reaction rates in the graphite and only the data from the 0.5-inch O.D. round copper foils was usable and indicated slight variation in the reaction rates of the copper foils at the cell boundaries with respect to the particle size of the fuel in the center cells during the irradiation.

2. Separable Foil Holding Fuel Rods

Sets of two 20-inch UO_2-2 wt% PuO_2 (8% ^{240}Pu) fuel rods were manufactured as separable units to contain the

Table IV. Relative Activities and Radial Location of Copper Foils Irradiated in Center Test Cell

Cell #	Traverse Position Ref*	Radius (in)	Measured Relative Count Rate Total	Epi Cadmium
I	R_1 (pins)	1.64	12.55 ± 0.5%	1.21 ± 1.0%
	R_2	1.12	12.44	1.22
	R_3	0.60	11.84	1.36
	R_4	0.60	11.98	1.37
	R_5	1.09	12.58	1.24
	R_6	1.59	12.88	1.21
	R_7	2.09	12.93	1.20
II	R_8	2.64	13.12	1.20
	R_9	2.13	13.08	-
	R_{10}	1.62	12.91	1.21
	R_{11}	1.11	12.95	1.20
	R_{12}	0.60	11.87	1.35
	R_{13}	0.61	11.76	1.36
	R_{14}	1.11	12.39	1.20
	R_{15}	1.63	12.59	1.18
III	R_{16}	2.11	12.71	1.16
	R_{17}	1.60	12.65	1.21
	R_{18}	1.08	12.50	-
	R_{19}	0.59	11.94	1.35
	R_{20}	0.59	11.41	1.35
	R_{21}	1.07	12.67	1.28
	R_{22}	1.58	12.95	1.23
	R_{23}	2.08	13.13	1.27
	R_{24}	2.58	13.13	1.19
IV	R_{25} (foils)	1.99	12.82	1.28
	R_{26}	1.21	12.66	1.28
	R_{27}	0.81	12.11	1.28
	R_{28}	0.81	12.12	1.28
	R_{29}	1.21	12.99	1.29
	R_{30}	1.81	13.20	1.29

*Figure 7, page 27.

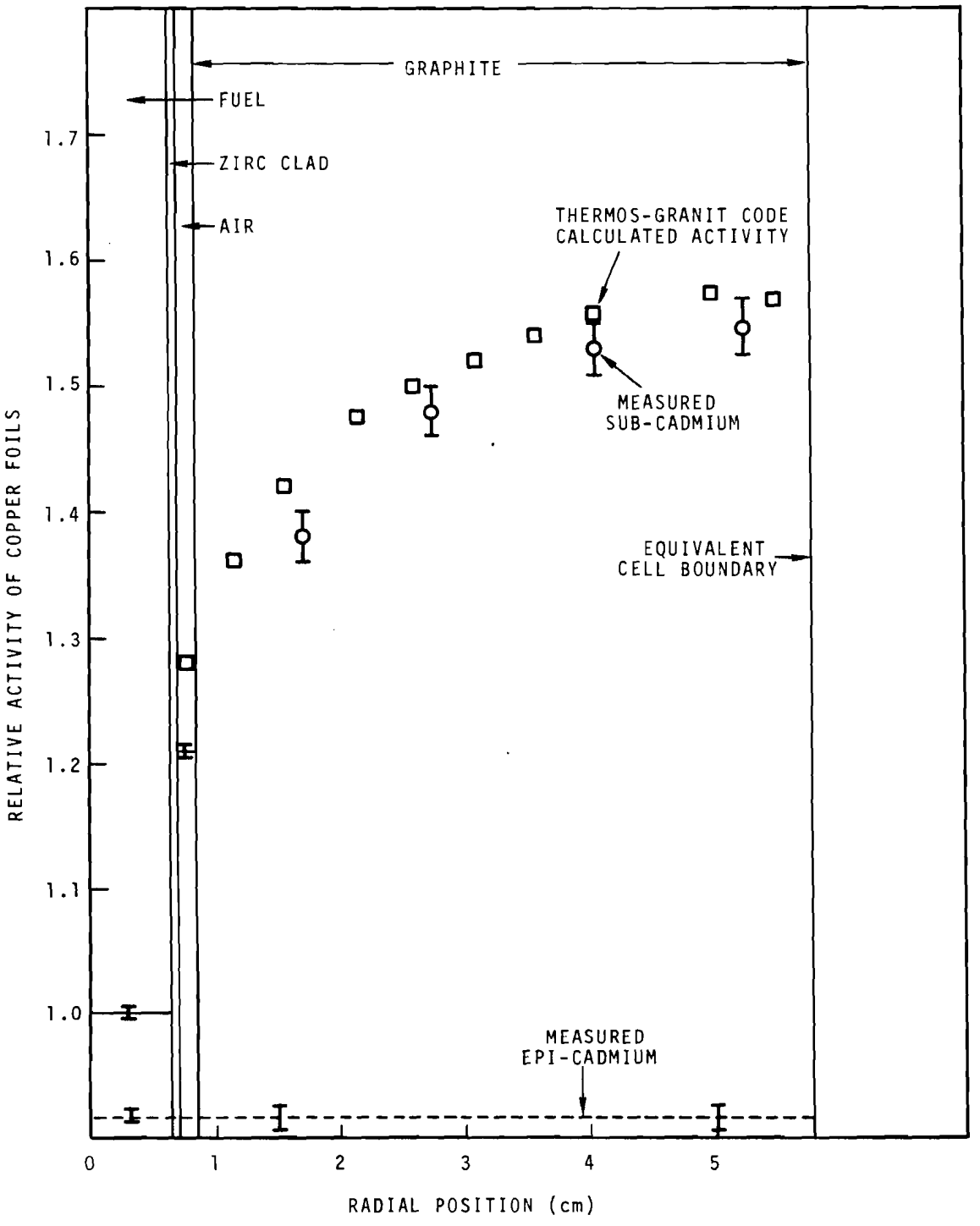

Figure 8. Measured vs Calculated Relative Reaction Rates of Copper Foils in Center Test Cells with Solid Solution Rods

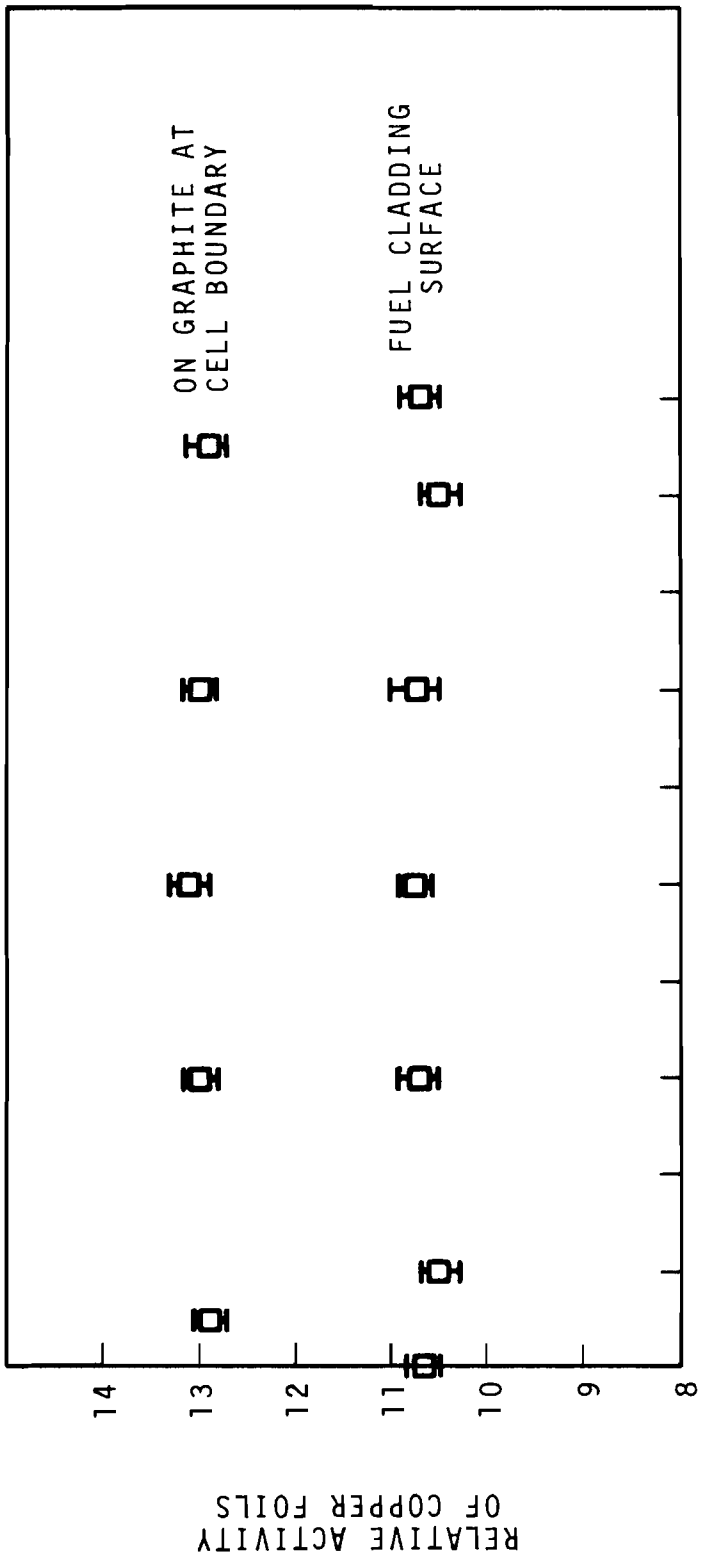

Figure 9. Axial Flux Traverse from Relative Copper Foil Measurement Along Center at Cell

3. Description of the Foils Containing Particulate Fuel

Special plutonium foils were fabricated for the measurements in the 330 micron particle fuel rods. Aluminum discs (0.5-inch O.D.) were drilled with holes, each one sufficiently small to contain a single 0.014-inch diameter PuO_2 particle. Each disc could contain approximately 45 particles. After insertion of the particles, the discs were clad in 0.005-inch thick aluminum covers. A diagram of the particle containing foils with respect to the particle containing rods is shown in Figure 11.

4. Description of Other Fission Foils

The plutonium reaction rate measurements in the solid solution rods were determined from a homogeneous foil of aluminum - 1.8 wt% Pu, also enclosed in a 0.005-inch thick aluminum cover as depicted in Figure 12.

The ^{235}U reaction rates were determined from homogeneous foils of aluminum - 7 wt% ^{235}U similar to the aluminum-plutonium foils but without the aluminum covers. Correction for the foil perturbations (discussed in the following section) were applied to the measured reaction rates.

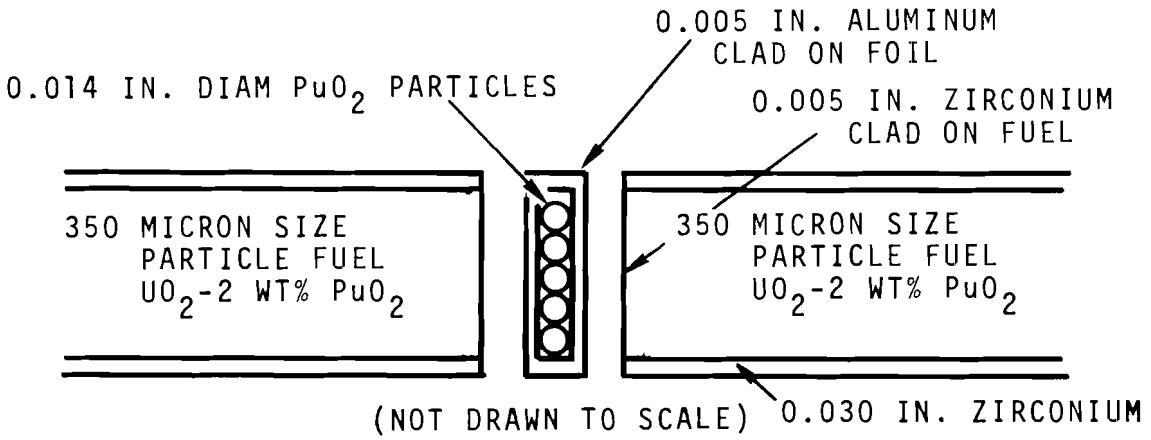

Figure 11. Diagram of Particle Foils and Particle Fuel

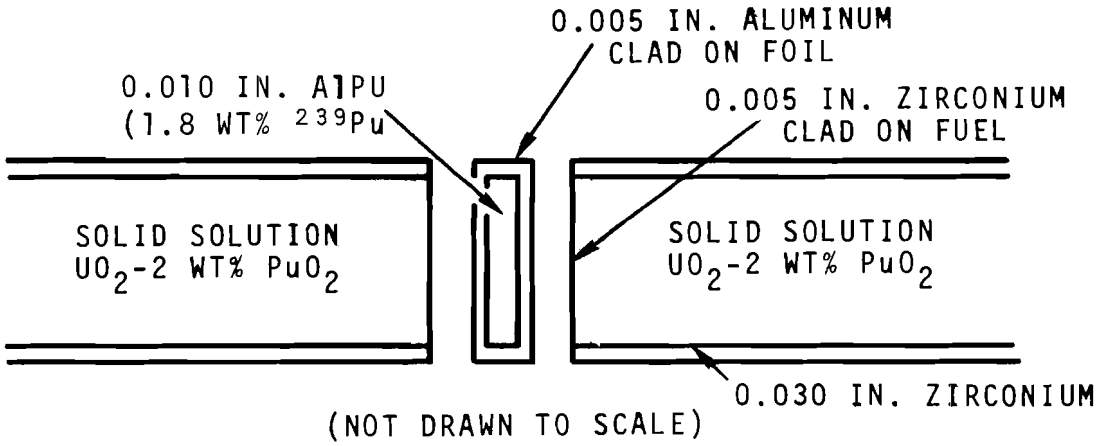

Figure 12. Diagram of AlPu Foils and Solid Solution Fuel

The parameters of all of these foil types are as follows:

Al-Pu	Plutonium and aluminum alloy mixture with 1.84 wt% Pu (8% ^{240}Pu) encased in an aluminum covering. Foils are approximately 0.010 inches thick, 0.5 inches O. D. and net weight is ∿0.08 grams.
Copper.	Copper discs 0.5 inch O.D. and 0.005 inches thick.
UAl	^{235}Uranium and aluminum alloy mixture in foils 0.5 inch O.D. and 0.003 inches thick (7 wt% ^{235}U).
330 Micron Particles.	Wafers of aluminum were drilled with ∿48 separate holes to contain spheroids of PuO_2 strategically picked and inserted by a jeweler. The holders were then sealed in an aluminum container.

5. Corrections to Foil Data

The photo peak radiation from a foil material irradiated at a point (r) in the reactor cell and measured by an appropriate detector and counting instrument with efficiency ε, can be defined by the following equation:

$$RR_{(r)} = \varepsilon \int^{\infty} N_i \sigma_{ai} (E)\ \mathbb{0}\ (E)\ dE$$

where $RR_{(r)}$ is the reaction rate of the foil material

N_i = Isotopic density of isotope i in material

σ_{ai} = Cross section of isotope i

$\mathbb{0}$ = Flux

E = Neutron energy

The terms of primary interest to these measurements are $\sigma(E,r)$ and $\phi\ (E,r)$ which can be used to derive the reaction rates of the materials in the cell. Most of the other terms can be normalized out by irradiating a similar foil in the PCTR thermal column[10] and counting both foils on the same counting systems so that it is possible to have relative count rates in the experimental analysis. Likewise the presence of the foil in the cell causes a perturbation in the flux which must be estimated and used as a correction to the measured data. These corrections require lengthy measurements and calculations which are described below. Their accuracy is important to the correct determination of self-shielding effects of the particles in the fuel in which the parameters of cross section (σ) and flux (ϕ) are different.

a. Mass Normalization Measurements

Prior to the experiment, the sets of fission foils containing similar fissionable material were irradiated simultaneously on the graphite rotator in the PCTR thermal column[10]. The flux in the thermal column is sufficiently constant that any differences in count rates can be attributed to differences in the amount of fissile material in the foils, provided the foils are of similar geometry and material[28]. This method was used to determine the relative mass of each set of fission foils used in the experiment.

Because the foil masses are on the order of two to three milligrams it is important that the mass of the foils used in the irradiations be known quite accurately to determine self-shielding effects in the plutonium. The foils containing the 330 micron particles were recently manufactured and the fissionable material accurately weighed. The Al-Pu foils were manufactured approximately eight years before this experiment and therefore it was deemed necessary to insure that the masses were correct. Therefore, one foil with listed weight as 1.656 grams Pu/foil, was chosen for chemistry analysis[12] and the results are listed in Table V.

Table V. Results From Chemical Analysis of Al-Pu Foil #3

	Lab Serial Number		
	3808-1	3808-2	Average
Pu (grams/foil)	1.667×10^{-3} ±1.5%	1.662×10^{-3} ±1.5%	1.665×10^{-3} ±1.5%
	Mass Spectrograph Analysis		
Pu Isotopic			
^{238}Pu wt%	.008 ± 2%	.007 ± 2%	.007 ± 2%
^{239}Pu wt%	94.380 ± 0.5%	94.395 ± 0.5%	94.385 ± 0.5%
^{240}Pu wt%	5.375 ± 0.5%	5.364 ± 0.5%	5.370 ± 0.5%
^{241}Pu wt%	.225 ± 1.0%	.225 ± 1.0%	.225 ± 1.0%
^{242}Pu wt%	.0124 ± 2.0%	.0127 ± 2.0%	.0126 ± 2.0%

*Average of duplicate aliquots 3808-1 and 3808-2 analyzed.

Significant figures as reported by Mass Spectrograph group.

Date of Analysis: March, 1970

b. Correction for Flux Peaking and Dipping

In reality the flux in the location of the foil is perturbed by the presence of the foil during the measurement. In a fuel rod, the flux tends to peak because the aluminum containing the fissionable material of the foil is not as black as the fuel material around the foil. In the thermal column or in the graphite moderator regions the flux will dip slightly because the foil material is usually a stronger neutron absorber than the material around the foil. Therefore, a new method was devised in this experiment to correct the foil data for these effects by calculating the flux dipping and/or peaking effects. R-Z geometry transport theory calculations were performed for the foil and fuel diagrams depicted in Figure 11 and 12 using the DOTSN[13] code. The sub-cadmium cross sections for the DOT Code were calculated from THERMOS[14] for the solid solution rods and with the GRANIT[15] code for the fuel rods. The epi-thermal cross sections were calculated using the EGGNIT-GRAINS Code[16].

Essentially, the flux enhancement factor due to the presence of the foil in the fuel was obtained

from the calculated ratio of the integrated flux in the foil area to integrated flux calculated in a similar geometry but with fuel material in place of the foil material. Thus, the correction factors for bare foils irradiated in the fuel can be defined as:

$$\frac{A_o}{A_{foil}} = \frac{(\bar{\sigma}_{th}\,\bar{\Phi}_{th} + \bar{\sigma}_{epi}\,\bar{\Phi}_{epi})_{fuel\ region}}{(\bar{\sigma}_{th}\,\bar{\Phi}_{th} + \bar{\sigma}_{epi}\,\bar{\Phi}_{epi})_{foil\ region}} \qquad (1)$$

where: A_o = the activity of the foil if the flux in the area were not affected by the presence of the foil

A_{foil} = measured foil activity

Φ_{fuel} = integrated flux in foil region calculated by DOTSN with fuel materials in all regions

Φ_{foil} = integrated flux in foil region calculated by DOTSN with foil and other materials as defined in Figures 10 and 11.

Similar R-Z calculations were also done for the copper foils and the Aluminum - 7 wt% ^{235}U foils irradiated in the fuel to obtain the flux peaking corrections for these foils.

6. Irradiation and Foil Analysis Techniques

As stated previously, only two rods in each set of four were separable. A foil containing ^{239}Pu fuel was placed in one of the rods, a copper foil and a foil containing ^{235}U were placed in the second rod, and all foils were irradiated simultaneously. Similar foils were irradiated in the PCTR thermal column for normalization purposes.

The initial irradiations were done with bare foils, followed by irradiations with cadmium (0.040-inch thick) covering the foils in the separable rods. The foils in the PCTR thermal column were always irradiated bare.

Each irradiation lasted two hours at a power level of 100 watts. Counting started eight hours after the irradiations so that the short-lived fission products had decayed to a negligible level. With only six foils per irradiation, the foils could be counted for a sufficient time and frequently enough that excellent counting data were obtained. Upwards of 10^5 counts were obtained from the bare foils and 10^4 counts were obtained from the cadmium covered foils.

The fission product decay gamma rays from the fission foils and the copper-64 decay gamma rays from the copper

foils were counted using a sodium iodide detector and associated digital counting equipment. The energy discriminator was set to eliminate all counts from gamma rays with energy less than 600 kev.

The unmodified relative foil activities were derived with respect to the foil activity in the thermal column by using the foil analysis code APDAC[11]. This code corrects the data for background, subtracts residual counts derived by counting the fission foils before the irradiation, corrects for mass differences, and decay time, and calculates the activation rates with respect to the thermal column foil with a statistical analysis of the results.

7. Measured and Calculated Reaction Rates With Respect to Particle Size

The self-shielding factors are defined as follows:

$$\frac{(\Sigma a \phi V)^{ss}_{Pu} - (\Sigma a \phi V)^{350}_{Pu}}{\Sigma a \phi V^{ss}_{Pu}} \qquad (2)$$

These terms were derived by the measured foil data and they were calculated by THERMOS[16] and GRANIT[17] computer codes.

a. Measured Results

The measured relative activity of the foils irradiated in the separable rods are listed in

Tables VI, VII and VIII for the plutonium, uranium and copper foils, respectively. The interpolated activities are also listed for similar foil types in the 50, 100 and 200 micron rods, assuming a linear self-shielding effect which is predicted by Thermos-Granit in the range of particle sizes being studied.

According to R. A. Lewis and T. J. Connally[2] this is a proper conclusion for cases in which the volume fraction (Va) of particles is sufficiently small to allow effectively uniform distribution of the particles (Va <0.03) and particle diameters up to 700 microns. The volume fraction for the fuels used in this experiment are approximately 0.02. Lane, Nordheim and Sampson[1] predict linear particle self-shielding effects as a function of grain diameter for particle sizes up to 600 microns.

8. Calculated Reaction Rates and Self-Shielding Effects

The experimental lattice cells were mocked-up in cylindrical geometry for calculation using the THERMOS and GRANIT Code which uses a special geometry routine to treat finite resonance shielding of particles embedded in cylindrical media by the method of Lane, Nordheim and

Table VI. Relative Plutonium Foil Activities With Respect to PuO_2 Particle Size

Particle Size Relative Activity	Solid Solution	Microns 50	110	200	330
		Interpolated Values			
Sub Cadmium	10.37 ±0.10	10.09	9.81	9.26	8.42 ±0.14
Epi Cadmium	0.564 ±0.006	0.559	0.555	0.546	0.533 ±0.009
Total	10.93 ±0.08	10.65	10.37	9.85	8.95 ±0.14

Table VII. Relative ^{235}U Foil Activities With Respect to PuO_2 Particle Size

Particle Size Relative Activity	Solid Solution	Microns 50	110	200	330
		Interpolated Values			
Sub Cadmium	7.64 ±0.05	7.69	7.74	7.84	7.99 ±0.05
Epi Cadmium	0.666 ±0.006	0.665	0.664	0.662	0.658 ±0.006
Total	8.30 ±0.04	8.35	8.40	8.50	8.65 ±0.05

Table VIII. Relative Copper Foil Activities With Respect to PuO_2 Particle Size

Particle Size Relative Activity	Solid Solution	Microns 50	110	200	330
		Interpolated Values			
Sub Cadmium	7.777 ±0.037	7.825	7.873	7.970	8.115 ±0.039
Epi Cadmium	1.247 ±0.010	1.247	1.247	1.236	1.245 ±0.010
Total	9.024 ±0.036	9.072	9.120	9.216	9.360 ±0.038

Sampson[17]. The relative reaction rates of the fissionable isotopes, ^{235}U and ^{239}Pu were calculated for five different particle sizes; namely, solid solution, 50 micron, 100 micron, 200 micron and 350 micron, respectively, in order to derive a functional description of the reaction rates with respect to particle size.

It must be noted that the code GRANIT does a two region calculation in the fuel of which one region represents the diluent (UO_2) and the other region the particulate material (PuO_2). Therefore uranium to plutonium ratios are no longer independent of the fuel flux average and the absorption rates in each calculation are not comparable without a normalization. Therefore the calculated reaction rates for each isotope with respect to particule size were normalized to equivalent average fluxes in the UO_2 fuel region, otherwise the relative absorption rates would have been calculated for different neutron densities.

In order to compare calculated versus measured attenuation factors, the calculated quantities were changed by a factor equal to the ratio of the copper foil activity in the particulate rod to the copper foil activity in the solid solution rod. This factor was assumed to be equivalent to the ratio of the flux

depression in the different rods due to particle effects.

The measured and calculated self-shielding effects[18] are illustrated in Figure 13 and Figure 14 for the plutonium and uranium, respectively. It is easy to perceive that as the particle lattice becomes more black to the neutrons the reaction rate in the other components of the cell increase. This is proven in the measurements and in the GRANIT calculation.

C. Analysis of Enrichment Content by Gamma Scanning

The measured self-shielding effect in the 330 micron PuO_2 particles were not compatible with the reactivity worths of the cells measured in the PCTR. If the plutonium was self-shielding as the foil data indicated, then the reactivity worths of the particle rods should have measured less than the reactivity worths of the solid solution rods. The experimental data (Table I) indicated the 330 micron particle rods to be almost as reactive as the solid solution rods. Likewise, sufficient data had been obtained so that it was possible to determine the infinite medium neutron multiplication as a function of the measured reaction rates. The results were in disagreement with the trends calculated in that the measured multiplication factors increased as the particle size increased. Therefore, steps were taken to resolve these contradictions.

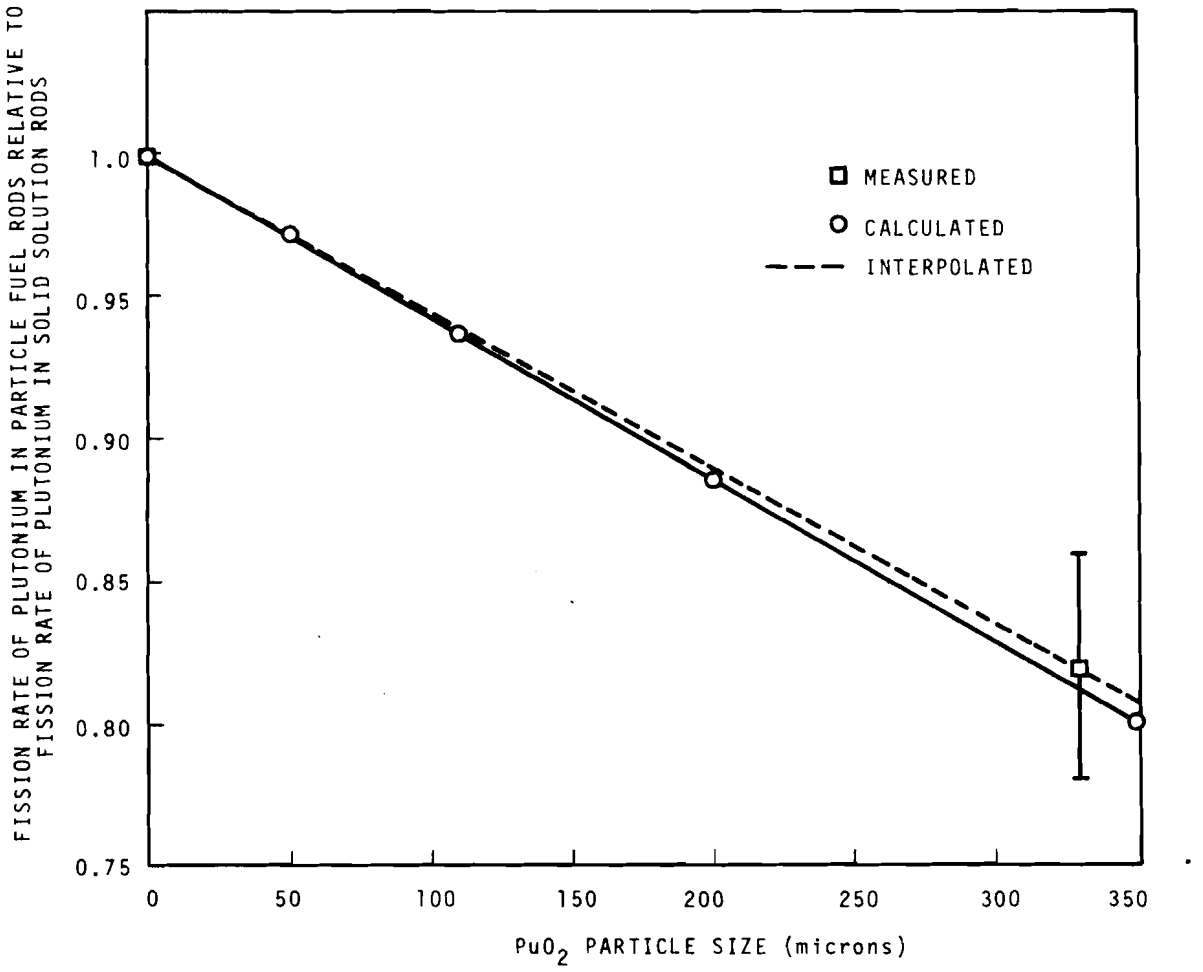

Figure 13. Comparison of Calculated and Measured Self Shielding Effects in Plutonium with Respect to Particle Size

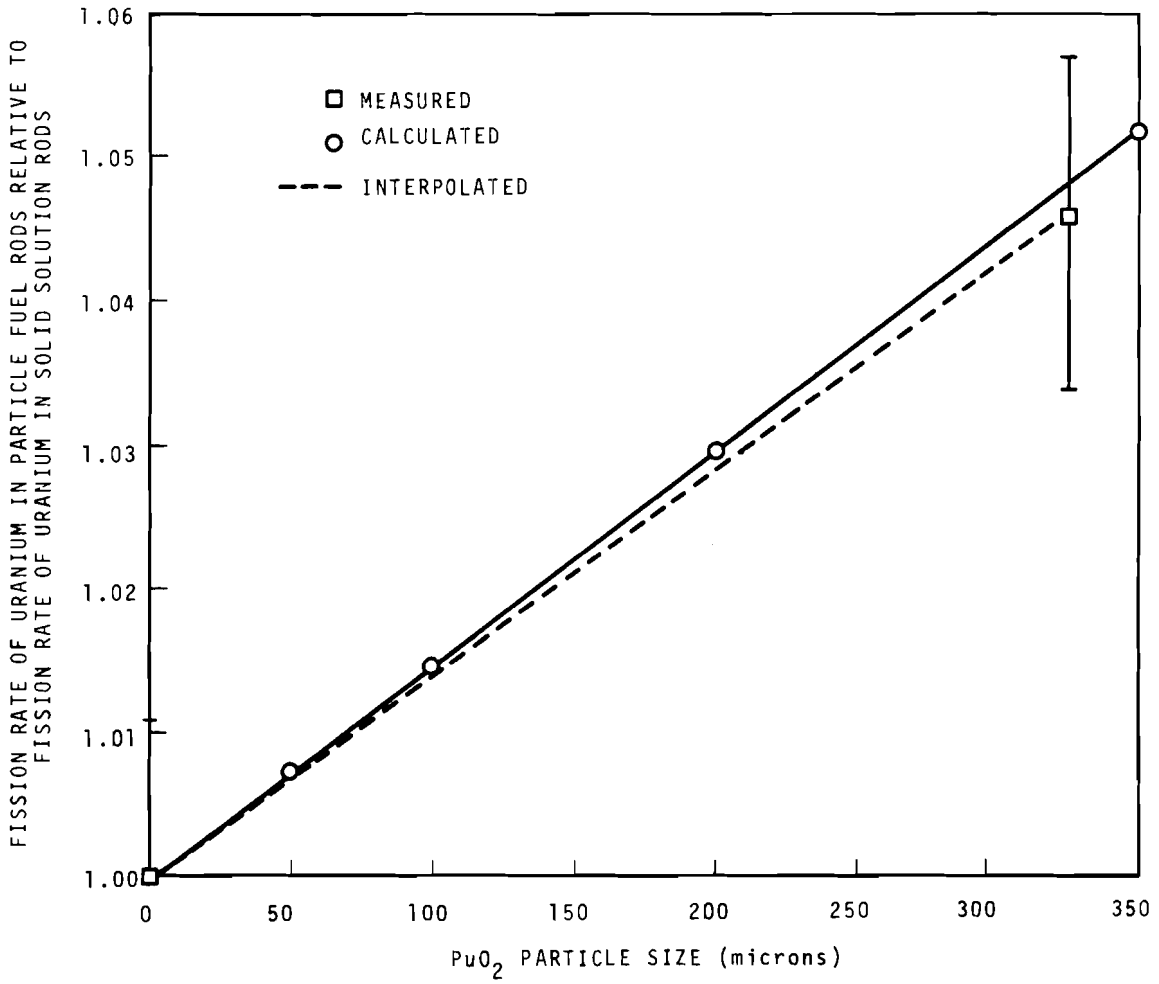

Figure 14. Comparison of Calculated and Measured Self Shielding Effects in Uranium with Respect to Particle Size Fuel Rods of UO_2-PuO_2

1. Chemistry Analysis

After the reactivity measurements were repeated in the PCTR, with the same results being obtained, it was suspected that there may be some other variation in the rods affecting the reactivities other than the particle effects. Therefore, one of the solid solution rods and one of the 330 micron particle fuel rods (both manufactured by the same methods) were opened and two pellets were removed from each rod. The four pellets were dissolved separately and analyzed for their plutonium content.

The results of the chemistry analysis are listed in Table IX. It is apparent from the chemistry samples that there could be as much as 20 percent difference between rods and ten percent difference between pellets. The scanning data seemed to indicate the same degrees of variation in the 330 micron particle rods; however, the scanning data for the other rods showed pellet differences of approximately five percent which is close to the statistical errors in the count rates.

2. Gamma Scanning

After receiving confirmation of the suspected enrichment variations in the fuel rods, a non-destructive analysis method was used to determine the enrichment variations in all the rods using gamma-ray techniques.

Table IX. Results From Analysis of UO_2-PuO_2 Fuel Rod Specimens[19]

Rod Type	8BMB Solid Solution		8B350 350 Micron Particles	
Pellet #	#1	#2	#1	#2
Pu/U (wt ratio)	0.0202 ±.0001	0.0202 ±.0001	0.0229 ±.00015	0.0249 ±.00015
wt% Pu (Pu + U)	0.0198 ±.0001	0.0198 ±.0001	0.0224 ±.00015	0.0243 ±.00015

Average Pu Isotopic Composition (All samples agreed within accuracy of measurement)

Pu-238 wt% (Pu)	0.0340	±.0035
Pu-239 wt% (Pu)	90.8524	±.0200
Pu-240 wt% (Pu)	7.9847	±.0200
Pu-241 wt% (Pu)	1.0687	±.0050
Pu-242 wt% (Pu)	0.0602	±.0018

U Isotopic Composition

U-234 wt% (U)	0.0054	±.0001
U-235 wt% (U)	0.7138	±.0002
U-238 wt% (U)	99.2808	±.0002

Date of Analysis: March, 1970.

The thermal absorption rates in ^{239}Pu, ^{235}U and ^{241}Pu can be inferred from the measured thermal fission rates using calculated values for α.

α = capture to fission ratio = $(\sigma_a - \sigma_f)/\sigma_f$.

This value for α was calculated using the GRANIT code and averaged over the test lattice fuel region.

$\underline{UO_2\text{-}2\ wt\%\ PuO_2\ RODS}$ (Solid Solution)

$$A_{th}^{239} = \left(\bar{\alpha}_{\substack{fuel \\ GRANIT}}^{239}\right)^{S.S.} \left[\left\{ \frac{SA_{fuel}^{239\ bare}}{SA^{239}_{\substack{Thermal \\ Column}}} \right\} \left(\frac{A_o}{A_{foil}} \right)^{\left(\substack{bare \\ AlPu}\right)}_{fuel} - \left\{ \frac{SA_{fuel}^{239\ cd}}{SA^{239}_{\substack{thermal \\ column}}} \right\} \left(\frac{A_o}{A_{foil}} \right)^{\left(\substack{Cd \\ PuAl}\right)}_{fuel} \right]_{\left(\substack{AlPu \\ foils}\right)} \sigma_{f_o}^{239} \left[g_f^{239} \left(\substack{thermal \\ column}\right) \right]_{THERMOS} \quad (12)$$

$$N^{239} V_{fuel} \left(\frac{A_{foil}}{A_o} \right)^{AlPu}_{\substack{thermal \\ column}}$$

Similar equations can be written for ^{235}U and ^{241}Pu. The thermal absorption rate for ^{240}Pu, ^{242}Pu, ^{238}U, Zr, H_2O, C, N and O can be inferred from the Cu activation data.

The method involved devising a system to measure gamma-ray photo peaks emitted by the plutonium isotopes. Initially, experiments were performed in which plutonium photo peaks were measured on a rather fundamental system to determine if there were differences in specific peaks measured from an SS rod in comparison to a 350 micron rod. When the initial results indicated certain photo peaks did vary and these variations corresponded to the chemistry measurements, the project was turned towards improving the counting system.

A high resolution germanium lithium detector system was set up to scan the rods at strategic axial locations while rotating the rod at 1 rpm. A diagram of the detector and the fuel rod system used in the scanning is illustrated in Figure 15.

The data was collected on a 4096 channel analyzer; however, only 500 channels were required because the data beyond 250 keV was not used. The channel energy width was set at 0.49 keV per channel. The analyzer data was printed out by a teletypewriter and also on punched paper tape. The typewriter data was transferred to punched cards by key-punch operators.

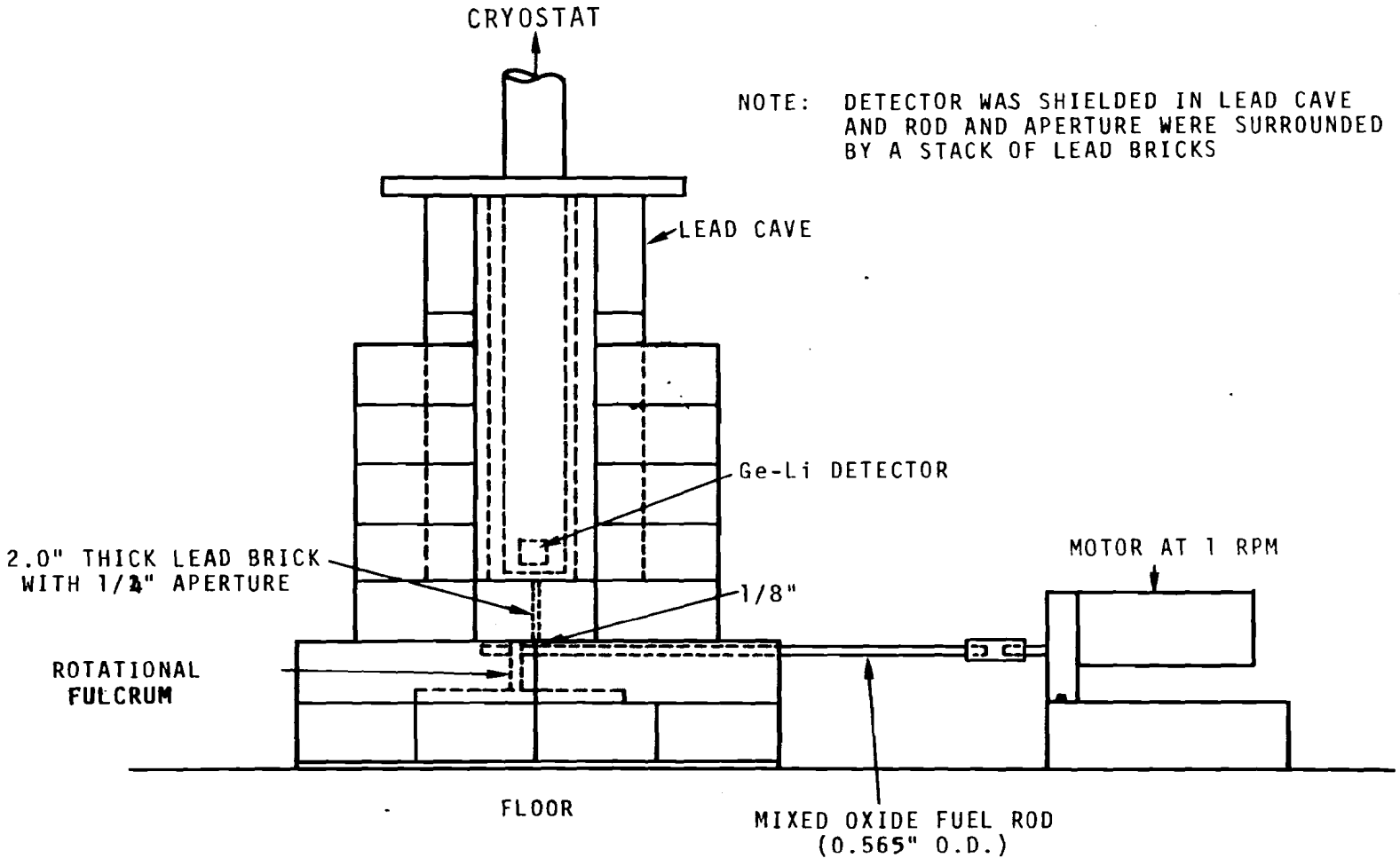

DIODE SIZE = 1x3x3 cm
APERTURE SIZE = 1/4" x 5/8"

Figure 15. Ge-Li Detector System to Determine Enrichment in Mixed Oxide Fuel Rods

One sample rod was chosen from each set of rods listed in Table I. It was assumed that the fuel enrichment in any single rod of a four rod set was the same as that in the other rods of the set. This assumption was partially tested during the PCTR reactivity measurements in which single rods of a particular particle and manufacturing technique were calibrated against the other three rods in the same set and no significant reactivity differences could be measured ($\leq 0.02¢$).

Minimum count times were six hours and were extended to eleven hours during the night. The equipment was calibrated at the start of each day by using a 137-Cesium gamma-ray source and no serious drift was ever detected.

The initial measurement goal was to take a separate scanning measurement on all the rods at a minimum of three axial locations; namely, 4.425, 9.425, and 14.425 inches which would place the aperture at the center of a single pellet in the rod. After the three measurements were taken on each rod, additional measurements were made on as many rods as possible by starting at 2.425 inches and moving the scanning point at two inch intervals until 10 separate scans had been completed.

The computer was used to analyze and to graph the scanning data. A graphic presentation of the scanning

data from one of the ball-milled solid solution rods, scanned at 9.425 inches from the end for 660 minutes is illustrated in Figure 16.

The gamma ray photo peaks which were selected for the enrichment analysis are listed below:

Isotope	$\bar{E}$ (keV)
$^{(20)}$Am-241	59.5
$^{(20)}$Pu-239	129.3
$^{(21)}$Pu-241	148.0
$^{(20)}$U-237	208.0

These peaks were chosen because they are relatively distinct photo peaks with an acceptable half-life and a reasonably clear shape of the spectrum and background in the adjacent energy range.

For the data analysis it was necessary to determine the areas of the peaks of interest. An analysis method was used in which the channels corresponding to the peak were summed and the average content of the channels adjacent to the peak channels were used to derive an average background for each channel under the peak which was then subtracted from the original sum.

The following list defines the start and end of the channels which were included in the summation of counts necessary to derive areas under the specific peaks being

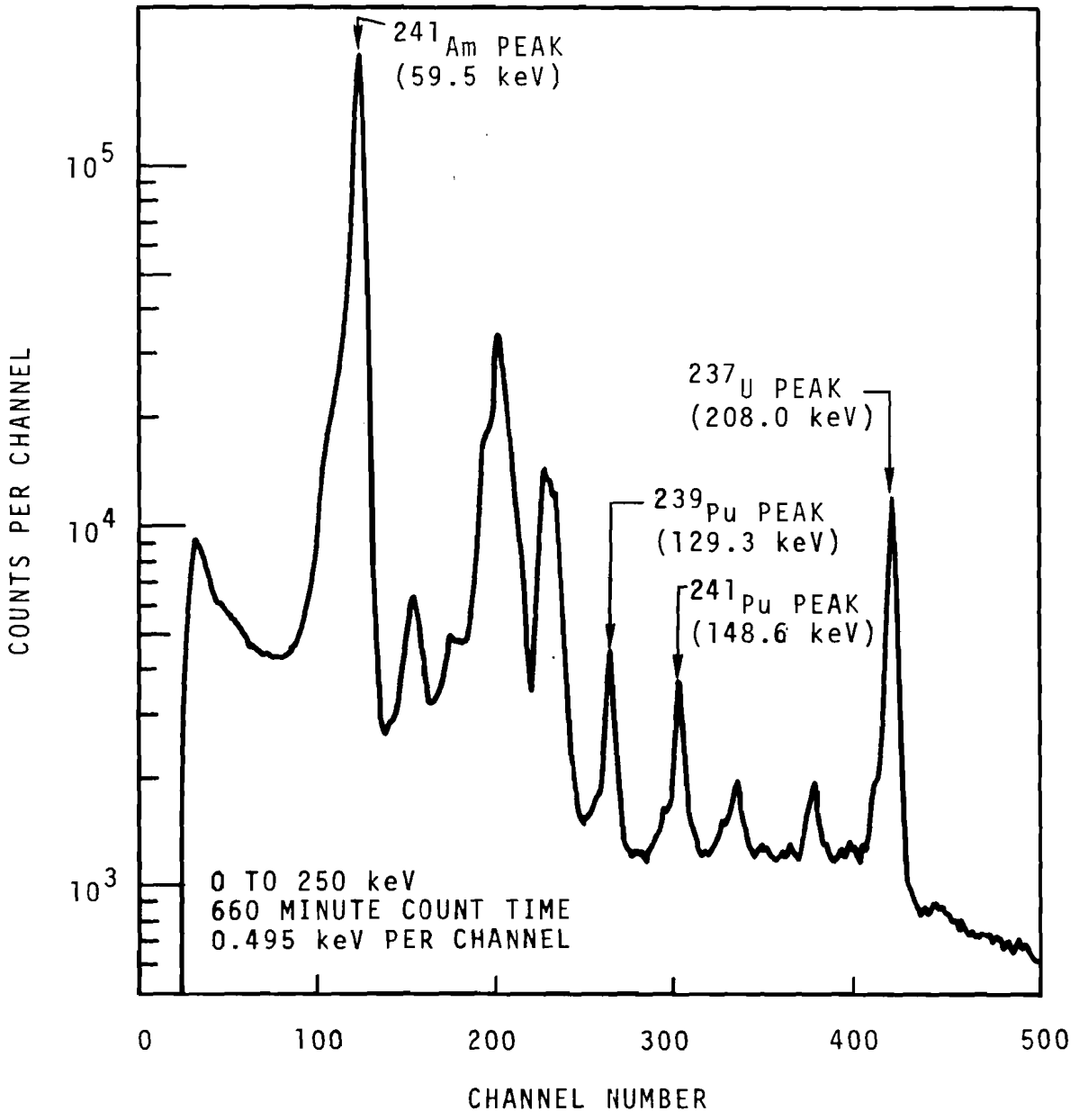

Figure 16. Graphic Presentation of Photo Peaks Measured During Scanning of Mixed Oxide Fuel Rod 8BMB

analyzed. The average number of background counts per channel was derived by averaging the counts in the four channel adjacent to the start and ending channels included in the peak.

- Channel 110 to 133 - 59.5 keV peak
- Channel 256 to 267 - 129.3 keV peak
- Channel 296 to 305 - 148.6 keV peak
- Channel 414 to 424 - 208.0 keV peak

The results of this data analysis are listed in Table X. The tabulated counts for each peak do not include the background and have been normalized to an equivalent counting live time.

From Table X data the following conclusions seem apparent:

- The 59.5 keV indicator is probably contaminated with lower energy gammas. Figure 3 also illustrates more than one peak may be involved.
- The rods 8SC and 8RA350 have similar isotopic ratios with lower 241:239 values.
- Rod 8BME has a significantly higher 241-239 ratio; however, only three scans were taken on the rod and the data could be inconclusive.
- The other rods have the same 241-239 ratios within the measurement accuracy (±3.4%) and, therefore, probably have similar isotopic fractions.

Table X. Average Integrated Counts From Specific Photo Peaks With Respect To Mixed Oxide Particle Rod Sets

Rod Designator	Number of Scan Points	Average Number of Counts			
		59.3 kev Peak	129.3 keV Peak	148.6 kev Peak	208.0 kev Peak
8BMB	10	747780	8845	6491	33418
8SC	10	706267	9203	4269	22373
8BME	3	872343	9410	8400	43405
8P50	10	814458	10055	7425	38646
8P100	3	826287	10529	8060	41106
8B100	10	883852	10788	7888	40390
8P200	3	768842	10094	7689	40795
8B200	10	761653	9925	7459	39595
8B350	10	730002	9869	7443	40234
8RA350	10	701047	10218	4685	25719

Calculation of the attenuation coefficients[22] for plutonium-oxide and uranium-oxide indicated that differences in these parameters for the two materials could affect the gamma scanning data. In other words, the attenuation factors were also a function of particle shape and size.

The self absorption distance z of a sphere of radius R_o was derived using the method and tables of reference 23 to determine the attenuation coefficient μz as a function of the size of the particle. The correction factors for the respective gamma ray photo peaks in UO_2 and PuO_2 were assumed to be directly proportional to the differences in the integrated peak counts due to this attenuation. The calculation parameters and correction factors are listed in Table XI.

Furthermore, on the basis of analyzing the corrected data by taking the ratio of specific counts from each rod to counts at a similar energy for rod 8BMB the following conclusions were drawn:

- Except for the 59.5 keV peak, most of the ratio of counts between rods indicate the enrichment variations between the rods.

Table XI. Attenuation Factors and Correction to Integrated Photo Peaks

Energy (keV)	$R_{o_{-6}}$ (cm^{-6})	z (cm)	μz		$e^{-\mu z}$		Correction Factor
			PuO_2	UO_2	PuO_2	UO_2	
129.3	330	.00877	.35040	.26421	.76781	.91743	1.0900
129.3	200	.00535	.21364	.16161	.80764	.84078	1.0534
129.3	110	.00300	.11961	.09069	.88727	.91330	1.0293
129.3	51	.0026	.05875	.04384	.94294	.95711	1.0150
148.6	330	.00897	.23951	.18074	.78701	.83466	1.0605
148.6	200	.00543	.14490	.10967	.86511	.89613	1.0358
148.6	110	.00302	.08050	.06107	.92266	.94075	1.0196
148.6	51	.00148	.03942	.02944	.96134	.97099	1.0100
208.0	330	.00919	.10977	.08276	.89604	.97057	1.0274
208.0	200	.00551	.06578	.04977	.93633	.95145	1.0161
208.0	107	.00304	.03631	.02753	.96434	.97284	1.0088
208.0	51	.00148	.01772	.01328	.98243	.98686	1.0045

- The above is not true of the ratios 8SC/8BMB, 8RA350/8BMB, and 8BME/8BMB because the isotopic fractions are different.
- The ratio of peaks at 129.3 keV for rods 8SC, 8RA350 and 8BME is probably the only indication of enrichment variations between these rods.

Therefore, the scanning data was used to determine relative enrichment content in the rods by comparison of applicable counting data from a questionable rod to the counting data from rod 8BMB. Rob 8BMB was used as a standard because the chemical analysis of the pellets in this particular rod set were in agreement with the manufacturer's original specifications.

Specifically, the following method was used to establish the enrichment content. The peaks were given equal weighting in the derivation of the enrichment content. It was learned later that the use of the single 129.3 keV peak would have given the same enrichment within the variance of the measurement; however, the additional measurements were added assurance that the data was consistent.

- For rod 8BMB, 8P50, 8P100, 8B100, 8P200, 8B200, 8B350

$$N_{Pu}^{Rod\ i} = N_{Pu}^{8BMB} \times \frac{\frac{A_{129.3\ keV}^{Rod\ i}}{A_{129.3\ keV}^{8BMB}} + \frac{A_{148.0\ keV}^{Rod\ i}}{A_{148.0\ keV}^{8BMB}} + \frac{A_{208.0\ keV}^{Rod\ i}}{A_{208.0\ keV}^{Rod\ 8BMB}}}{3} \quad (3)$$

where N_{Pu} = atom density plutonium

A = integral scan data for specific peak energy

i = questionable rod

- For rods 8SC, 8RA350 and 8BME

$$N_{Pu}^{Rod\ i} = N_{Pu}^{8BMB} \times \frac{A_{129.3\ keV}^{Rod\ i}}{A_{129.3\ keV}^{8BMB}}$$

3. Conclusions Derived From Scanning Measurements

The determined weight fractions of plutonium in the rods are listed in Table XII with the relative reactivity worths measured in the PCTR.

From Table XII it is apparent that the rods were probably manufactured from three separate batches of fuel material. The differences in isotopic concentration coincide with the time and methods of production.

Rods 8SC and 8RA350 - These rods were the initial rods made for the experiment by the earlier methods and with very limited particle yields.

Rods 8BMB - These rods were manufactured within a
8P50
8B100 reasonably close time interval.
8P200
8B200
8B350

Table XII. Enrichment of PuO_2-UO_2 Particle Fuel Determined by Gamma Scanning, Chemistry, and Reactivity Measurements

Rod Designator	Rod Type	wt% PuO_2 (By Gamma Scanning)	Relative Reactivity Worth in PCTR	Chemical Analysis of Two Pellets (wt% PuO_2)	Density g/cc
8BMB	Solid solution	Used as base (1.98)	1.0	1.98	8.571
8SC	Solid solution	2.08 ±.08	1.043 ±.007	None	8.704
8BME	Solid solution	2.10 ±.09	1.018 ±.007	None	8.474
8P50	50 micron	2.29 ±.09	1.088 ±.007	None	8.601
8P100	110 micron	2.47 ±.10	1.074 ±.007	None	8.638
8B100	110 micron	2.48 ±.10	1.102 ±.007	None	8.739
8P200	200 micron	2.41 ±.08	1.030 ±.007	None	8.657
8B200	200 micron	2.35 ±.09	1.036 ±.007	None	8.718
8RA350	330 micron	2.47 ±.09	0.997 ±.007	None	8.798
8B350	330 micron	2.42 ±.09	0.981 ±.007	2.43	8.691

which will be presented in a section which follows.

1. Theoretical Calculation Methods and Programs

Two group calculations serve as the basis for theoretical analysis of the PuO_2 particle size experiments. Of primary importance to the conduct of these calculations is the correctness of cross section data and averaging techniques for transposing these data into the required two group constants. Basic cross section data utilized in the computations were acquired from the Battelle Master Library[24].

To compute a characteristic neutron spectrum for obtaining the required two-group constants, it is necessary to solve the Boltzmann transport equation by some approximate method since exact solutions are not economically feasible. The slowing down spectrum was computed using the EGGNIT[16] code which (1) incorporated spatial dependence by specification of a buckling independent of neutron energy, and (2) the angular flux dependence is simplified by application of the B_1 approximation[25]. Resonance self-shielding in both the particles and fuel assemblies were treated by the Nordheim integration technique for the stronger absorption lines and with the NR approximation for the weaker resonance[26].

An interaction technique has been incorporated into EGGNIT which treats resonance shielding for multi-annular regions and other complex geometries. A special geometry routine was written (GRAINS) to treat finite resonance shielding of particles embedded in a cylindrical media by the method of Lane, Nordheim, and Sampson[17].

The thermal group constants were calculated by a revised version of THERMOS[12], called GRANIT[13], which also applies the method of Lane, et al[17] for treating the thermal self-shielding in the fuel particles. The scattering kernels for carbon are basically Park's kernel computed with the SUMIT[27] code.

E. Determination of k_∞^* From The Null Reactivity Experimental Data

1. Theory Definition of k_∞^* In The Poisoned Lattice Technique

The term k^* is defined here as the multiplication factor of a neutron multiplying medium based primarily on the PCTR technique[28] of determining the excess neutron production of a test sample. This excess neutron production is deduced from the measured amount of neutron absorber that must be added to the test sample to obtain a null reactivity change when the test sample is compared with a void and reduces the buckling of the

poisoned central cell to zero. The expression using the experimentally derived parameters necessary for the determination of k_∞^* are listed below and the derivation is shown in Appendix C.

$$k^* = TP \times \frac{A_2' + A_{2a}' + p A_{1a}'}{TP'} \qquad (5)$$

where TP = total production of neutrons

A_2 = absorption of thermal neutrons in un-poisoned lattice cell

TP' = total production of neutrons in poisoned lattice cell

A_{1a}' = absorption of epi-thermal neutrons in mass of copper around lattice cell to achieve null reactivity

A_{2a}' = absorption of epi-thermal neutrons in mass of copper around lattice cell to achieve null reactivity

P = escape to thermal probability

The quantities in the simplified expression above are defined below with all the details of their measured and/or calculated parameters.

UO_2-2 wt% PuO_2 RODS (Solid Solution)

$$TP^{239} = \left[\frac{SA^{239}(\text{fuel})}{SA^{239}\left(\begin{matrix}\text{thermal}\\ \text{column}\end{matrix}\right)}\right]_{\left(\begin{matrix}\text{AlPu}\\ \text{foils}\end{matrix}\right)}^{\text{bare}} \nu\,\sigma_{fo}^{239}\left[g_f^{239}\left(\begin{matrix}\text{thermal}\\ \text{column}\end{matrix}\right)\right]_{\text{THERMOS}} N^{239} V_{\text{fuel}} \qquad (6)$$

$$\left[\left(\frac{A_{foil}}{A_o}\right)_{\text{thermal column}}^{(PuAl)} \left(\frac{A_o}{A_{foil}}\right)_{\text{fuel}}^{\text{bare}\ (AlPu)}\right]_{\text{DOT-SN}}$$

where

SA^{239}_{fuel} = measured activity of ^{239}Pu foil irradiated in fuel rod

$SA^{239}_{\substack{\text{thermal}\\ \text{column}}}$ = measured activity of ^{239}Pu foil irradiated in thermal column

σ^{239}_{fo} = fission cross section ^{239}Pu (2200 m/sec)

g_f^{239} = non 1/v factor for ^{239}Pu calculated by THERMOS.

N^{239} = nuclei density ^{239}Pu

V = volume fuel

$\frac{A_{foil}}{A_o}$ = flux dipping correction factor for fuel irradiated in thermal column (calculated by DOT-SN code)

$\frac{A_o}{A_{foil}}$ = flux peaking correction factor for foil irradiated in fuel (calculated by DOT-SN code)

$$TP^{235} = \left[\frac{SA^{235}(\text{fuel})}{SA^{235}\left(\begin{matrix}\text{thermal}\\ \text{column}\end{matrix}\right)}\right]_{\substack{\text{bare}\\ \text{UAl}\\ \text{foils}}} \nu\sigma_{fo}^{235}\left[g_f^{235}\left(\begin{matrix}\text{thermal}\\ \text{column}\end{matrix}\right)\right]_{\text{THERMOS}} \quad (7)$$

$$N^{235}V_{\text{fuel}}\left(\frac{A_{\text{foil}}}{A_o}\right)^{(\text{UAl})}_{\substack{\text{thermal}\\ \text{column}}}\left(\frac{A_o}{A_{\text{foil}}}\right)_{\substack{\text{DOT-SN}\\ \text{fuel}}}$$

where parameters are same as above except they apply to ^{235}U isotope.

Assume ^{241}Pu has same activation ratio as Pu^{239} (this is a very small term)

$$TP^{241} = \left[\frac{SA^{239}(\text{fuel})}{SA^{239}\left(\begin{matrix}\text{thermal}\\ \text{column}\end{matrix}\right)}\right]_{\substack{\text{bare}\\ \text{PuAl}\\ \text{foils}}} \nu\sigma_{fo}^{241}\left[g_f^{241}\left(\begin{matrix}\text{thermal}\\ \text{column}\end{matrix}\right)\right]_{\text{THERMOS}} \quad (8)$$

$$\left[N^{241}V_{\text{fuel}}\ \frac{A_{\text{foil}}}{A_o}\right]^{(\text{AlPu})}_{\substack{\text{thermal}\\ \text{column}}}\left(\frac{A_o}{A_{\text{foil}}}\right)^{\substack{\text{bare}\\ (\text{AlPu})}}_{\substack{\text{DOT-SN}\\ \text{fuel}}}$$

where quantities are same as above except for ^{241}Pu isotope.

$\underline{UO_2\text{-}2\ wt\%\ PuO_2\ RODS}$ (350μ PuO_2 Particles)

$$TP^{239} = \left[\frac{SA^{239}(fuel)}{SA^{239}\left(\begin{matrix}thermal\\column\end{matrix}\right)}\right]_{\begin{matrix}bare\\(350\ foils)\end{matrix}} \left(\frac{A_{foil}}{A_o}\right)_{\begin{matrix}thermal\\column\ GRANIT\end{matrix}} \tag{9}$$

$$\nu\sigma_{fo}^{239}\left[g_f^{239}\left(\begin{matrix}thermal\\column\end{matrix}\right)\right]_{THERMOS} \quad N^{239}V_{fuel}\left(\frac{A_o}{A_{foil}}\right)_{\begin{matrix}DOT\text{-}SN\\fuel\end{matrix}}$$

where quantities are same as listed above except the foil activities noted as 350 Pu apply to particle foils in fuel.

$$TP^{235} = \left[\frac{SA^{235}(fuel)}{SA^{235}\left(\begin{matrix}thermal\\column\end{matrix}\right)}\right]_{\begin{matrix}bare\\UAl\\foils\end{matrix}} \nu\sigma_{fo}^{235}\left[g_f^{235}\left(\begin{matrix}thermal\\column\end{matrix}\right)\right]_{THERMOS} \tag{10}$$

$$N^{235}V_{fuel}\left[\frac{A_{foil}}{A_o}\right]^{(UAl)}_{\begin{matrix}thermal\\column\end{matrix}} \left(\frac{A_o}{A_{foil}}\right)^{(UAl)}_{\begin{matrix}DOT\text{-}SN\\fuel\end{matrix}}$$

where quantities are same as listed above except for ^{235}U isotope. Assume ^{241}Pu has same activation ratio as ^{239}Pu (this is a very small term)

$$TP^{241} = \left[\frac{SA^{239}(fuel)}{SA^{239}\left(\begin{matrix}thermal\\column\end{matrix}\right)}\right]_{\begin{matrix}bare\\PuO_2\\foils\end{matrix}} \left(\frac{A_{foil}}{A_o}\right)^{PuO_2}_{\begin{matrix}thermal\\column\\GRANIT\end{matrix}} \tag{11}$$

$$\nu\sigma_{f_o}^{241}\left[g_f^{241}\left(\begin{matrix}thermal\\column\end{matrix}\right)\right]_{THERMOS} \quad N^{241}V_{fuel}\left(\frac{A_o}{A_{foil}}\right)^{\begin{matrix}bare\\PuO_2\end{matrix}}_{\begin{matrix}DOT\text{-}SN\\fuel\end{matrix}}$$

$$A_{th}^{238} = \left[\left(\frac{SA_{fuel}^{cu}}{SA^{cu}} \right)_{thermal\ column}^{bare} \left(\frac{A_o}{A_{foil}} \right)_{fuel}^{bare\ Cu} - \left(\frac{SA_{fuel}^{CuCd}}{SA^{Cu}_{thermal\ column}} \right) \right. \quad (13)$$

$$\left. \left(\frac{A_o}{A_{foil}} \right)_{fuel}^{Cd\ Cu} \right] \sigma_{a_o}^{238} \left[g_a^{238}{}_{fuel\ GRANIT} \right] N^{238} V_{fuel} \left(\frac{A_{foil}}{A_o} \right)_{thermal\ column}^{Cu}$$

Similar equations can be written for the other cell components.

2. Results (k* by Null Reactivity Technique)

The measured quantities which are necessary to the determination of k* by the null reactivity technique are listed in Table XIV. Normally the parameters measured by the null reactivity technique would define k* for all the rods but the enrichment variations among the particle rods which were not known at the time of the measurements, render the null reactivity data invalid. Therefore, no values of k* have been derived for those rod sets.

3. Normalization of Measured k_∞^* to Equivalent Fuel Density

For comparison purposes, the k_∞^* values were normalized to an equivalent fuel density by the following method. A

Table XIV. Measured Relative Production and Absorption Terms for the Derivation of k* by the Null Reactivity Method

Rod Designator	Enrichment wt%	TP	A2	TP′	A2′	A2a	pA1a	k^*_∞	k* (with density correction)
8BMB	1.98	10.2235	5.5998	3.7867	2.0559	1.0286	.0993	1.5350	1.5437
8SC	2.08	10.6010	5.7878	3.9274	2.1268	1.0759	.1038	1.5420	1.5440
8BME	2.10	10.7585	5.8533	3.9873	2.1521	1.0473	.1011	1.5214	1.5341
8P50	2.29	11.3097	6.1262	Data not applicable because of flux mismatch					
8B100	2.48	11.3875	6.1093	in null reactivity condition.					
8P100	2.47	11.4518	6.1701						
8B200	2.35	10.8784	5.9127						
8P200	2.41	11.1146	6.6260						
8B350	2.42	10.4085	5.6928						
8RA350	2.47	10.5482	5.7533						

set of low density fuel rods containing 100 micron PuO_2 particles were fabricated for the center cell. The mass of copper necessary to achieve unit multiplication was measured with these low density rods the same as for the other rods. Thus, a relationship was established which included the variations in copper neutron absorber requirements with respect to the density of the fuel. The correction method is shown as follows:

Mass of Copper Necessary to Achieve Unit Multiplication

- for 100 micron rod set 8B100	2006.3 gm cu.
- for 100 micron low density rods	1824.1 gm cu
- ΔMass	182.2 gm cu.
- Homogenized density 100 micron rods 8B100	8.73 gm/cc
- Homogenized density 100 micron low density rods	7.63 gm/cc
- ΔMass Cu/Δdensity of rod	164.24 gm cu/gm/cc
- Homogenized density solid solution rod set 8BMB	8.57 g/cc
- ΔM_o = 164.24 (8.739 - 8.570)	+ 27.60 gm cu.
- Measured M for set 8BMB	1823.5 gm cu.

- Correction factor for copper absorption $\frac{1823.5 + 27.60}{1823.5} = 1.014$

- Corrected k_∞^* $\frac{TP}{A_2} \times \frac{A_2' + 1.014(A_{1a}' + A_{2a}')}{TP'}$

$= 1.827 \times .844$

$= 1.543$

F. Determination of k_∞^* From The Adjoint Weighted Cross Section Technique (Unpoisoned Technique)

1. Theory-Definition of k* From The Unpoisoned Technique

The adjoint weighted cross section technique, also referred to as the unpoisoned technique is a means for obtaining k_∞^* from the ratio of the reactivity coefficients of a neutron multiplying sample and a normalizing thermal neutron absorber. The method makes use of the general perturbation expressions derived by Heineman[5]:

$$x\Delta\rho = \sum_i \int_S ds\, \phi_i^+ J_i' \qquad (14)$$

where

$$x = \sum_i \int_{Vo} dV \phi_i^+ \phi_i'^+ \qquad (15)$$

and S is the surface enclosing the test sample, Vo is the reactor volume exterior to the test sample, and J' is the outward normal current at the surface of the test sample.

Heineman's technique is a means of extending the null reactivity method to systems where the buckling is not adjusted to zero as it is in the null reactivity technique.

Lippincott, et al, show in Reference 28 that the following equation can be derived for k* when the measured parameters of the adjoint weighted cross section technique are included:

The expression for k_∞^* in the unpoisoned technique becomes

$$k_\infty^* = 1 - \frac{\Delta\rho_{cell}}{\Delta\rho} \frac{\left(\Sigma_2^a \phi_2 V\right)_p}{\left(\Sigma_2^a \phi_2 V\right)_{cell}} \left[1 + \frac{\phi_1^+}{\phi_2^+} \frac{\left(\Sigma_1^a \phi_1\right)_p}{\left(\Sigma_2^a \phi_2\right)_p}\right] \quad (16)$$

$$+ \frac{\tau B^2(1+B^2L^2)[\tau B^2 - v_1\Sigma_1^f/(\Sigma_1^R + \Sigma_1^a)]}{[1 + \tau B^2 - V_1\Sigma_1^f/(\Sigma_1^R + \Sigma_1^a)]}$$

If one substitutes $n_1 f_1 \Sigma_1^a$ for $v_1\Sigma_1^f$, the second part of the expression becomes

$$\frac{TB^2(1 + L^2B^2)\ [TB^2 - n_1 f_1(1-p)]}{1 + TB^2 - n_1 f_1(1-p)} \quad (17)$$

where

$\Delta\rho_{cell}$ = the reactivity worth of the test cell (measured)

$\Delta\rho_p$ = the reactivity worth of a copper sample in the empty test cell (measured)

$(\Sigma_2^a \phi_2 V)_{cell}$ = the relative absorption rate of the cell; this quantity is also determined for the null reactivity technique (measured) and was defined as A2.

$(\Sigma_2^a \phi_2 V)_p$ = the relative reaction rate of the copper poison used to measure the reactivity worth of copper ($\Delta\rho_p$).

$\frac{\phi_1^+}{\phi_2^+} \approx$ = escape to thermal probability calculated by EGGNIT-GRAINS code

$T+L^2$ = neutron age and diffusion length calculated by EGGNIT-GRAINS

B^2 = material buckling calculated by ANISN (29) using cross section from EGGNIT and THERMOS codes

2. Measured k_∞^* From Adjoint Weighted Cross Section Data

The k_∞^* which were measured in the unpoisoned experimental technique and defined as the infinite medium multiplication factor for the cell with leakage (as a cell in the just critical environment) are summarized in Table XV with respect to particle size. This table includes the parameters defined for equations (12) and (13), pages 72 and 73, which are the measurements necessary to this

Table XV. Measured and Calculated Quantities to Determine k* by Unpoisoned Method

	Fuel Designator									
	8BMB	8SC	8BME	8P50	8B100	8P100	8B200	8P200	8B350	8RA350
Particle Size	(Solid Solution)			50	110	110	200	200	330	330
Average reactivity per cell (¢)	37.590 ±.320	38.152 ±.330	37.858 ±.340	39.115 ±.330	39.292 ±.330	38.909 ±.330	38.258 ±.330	38.228 ±.330	37.321 ±.330	37.605 ±.330
Reactivity worth of copper in void (¢)	7.203 ±.020	7.203 ±.020	7.203 ±.020	7.203 ±.020	7.203 ±.020	7.203 ±.020	7.203 ±.020	7.203 ±.020	7.203 ±.020	7.203 ±.020
$(\Sigma\phi V)_2 = A_2$	5.703	5.809	5.854	6.126	6.109	6.170	5.913	6.026	5.693	5.733
$(\Sigma\phi V)_2^p = A_2'$	0.509	0.509	0.509	0.509	0.509	0.509	0.509	0.509	0.509	0.509
$(\Sigma\phi V)_1^p = A_1'$	0.054	0.054	0.054	0.054	0.054	0.054	0.054	0.054	0.054	0.054
p(EGGNIT CALC)	0.837	0.837	0.936	0.836	0.838	0.837	0.841	0.841	0.844	0.844
B^2(ANISN CALC)	8.79-4	8.79-4	9.03-4	9.22-4	9.36-4	9.41-4	9.41-4	9.15-4	9.05-4	9.05-4
T (age)	318.3	318.3	318.2	318.2	318.2	318.2	318.1	318.1	318.0	318.0
k(unpoisoned technique)	1.499 ±.010	1.496 ±.010	1.489 ±.010	1.482 ±.010	1.486 ±.010	1.476 ±.010	1.489 ±.010	1.479 ±.010	1.496 ±.010	1.494 ±.010
Correction to obtain k* of poisoned technique	.050	.050	.057	.059	.061	.062	.058	.059	.055	.055
Measured k* (unpoisoned technique)	1.549 ±.010	1.546 ±.010	1.546 ±.010	1.541 ±.010	1.547 ±.010	1.538 ±.010	1.547 ±.010	1.538 ±.010	1.551 ±.010	1.549 ±.010
k* (poisoned technique)	1.544 ±.011	1.534 ±.011	NA	NA	NA	NA	NA	NA	NA	NA
Enrichment wt% Pu	1.98	2.08	2.10	2.29	2.48	2.47	2.35	2.41	2.42	2.47

technique to determine ($\Sigma_2^a \phi V$) cell.

To verify the experimental technique, the k* which is measured in the null reactivity technique has been listed for the solid solution rod sets only. The enrichment differences which were unknown at the time of the measurements have rendered the null reactivity technique data invalid for proper use of this particular method except in the balanced spectrum. The spectrum was only matched for the case of the 2 wt% solid solution rods in the center cell.

The k_∞^* derived from the adjoint weighted cross technique measurements are listed in Table XV.

G. Comparison of Theory and Experiment

1. Definition of Theoretical k_∞'

The parameter of major interest obtained from the PCTR experiments is the infinite medium neutron multiplication factor which has been expressed as k_∞^* and is defined by the usual two group notation.

$$k^* = \frac{\nu\Sigma_{f1}\phi_1' + \nu\Sigma_{f2}\phi_2'}{\Sigma_{a1}\phi_1' + \Sigma_{a2}\phi_2'} \times P \quad \text{(18)}$$

where P is the escape to thermal probability

and the subscripts 1 and 2 denote the fast and thermal groups, respectively. The upper bound for the thermal group constants is 0.683 ev. One particular point of

emphasis is that ϕ_1' are neutron fluxes in equilibrium in the fundamental mode (just critical) environment and not those characteristics of an infinite medium.

The infinite medium neutron multiplication factor calculated by various theoretical models is defined as

$$k_\infty' = \frac{\text{Total neutron production}}{\text{Total neutron absorption}} = \frac{\nu_1 \Sigma_1^f \phi_1' + \nu_2 \Sigma_2^f \phi_2'}{\Sigma_1^a \phi_1' + \Sigma_2^a \phi_2'} \qquad (19)$$

where ϕ_1' and ϕ_2' equilibrium fluxes in the fundamental mode problem (a just critical sphere of the test material). C. R. Richey, et al[28] have derived the parameters or corrections necessary to compare the theoretical k_∞' with the measured k_∞^* as follows:

$$k' = k^* - \frac{(1 + \tau B^2)(1 + L^2 B^2)(1-p)L^2 B^2}{1 + (1-p)L^2 B^2} \qquad (20)$$

Physically, the difference between k_∞' and k_∞^*, says Lippincott, et al, "arises because k_∞^* does not take into account the fact that neutrons absorbed before being thermalized do not undergo thermal leakage. The value $k_\infty'-1$ represents the true number of neutrons that leak out of a bare critical reactor for each neutron (of any energy) absorbed in the reactor." Therefore, the above quantity (Equation 20) will be called a leakage correction in those tables which include numerical quantities of this parameter.

2. Derivation of Mis-Match Corrections for Unpoisoned Technique

However, if the fluxes and adjoints in the reactor which are used to measure the copper and cell worths are not matched, then the equation

$$k_\infty' = k_\infty^* - \frac{(1 + TB^2)(1 + L^2B^2)(1-p)L^2B^2}{1 + (1-p)L^2B^2} \qquad (21)$$

is not complete and we must denote the actual reactor fluxes and adjoints by primed equations and the equations using the poison technique as an example:

$$\frac{\Delta\rho_{cell}}{\Delta\rho_p} \frac{(\Sigma_2\phi_2 V)p}{(\Sigma_2^a\phi_2 V)_{cell}} = 1 + \frac{\Sigma_1^p\phi_1^p\phi_1^+}{\Sigma_2^p\phi_2^p\phi_2^+} = \frac{D_2\nabla^2\phi_2'}{\Sigma_2^a\phi_2'} - \frac{D_1\nabla^2\phi_1'\phi_1'^+}{\Sigma_2^a\phi_2'\phi_2'^+} \qquad (22)$$

Lippincott[30] has shown that the total expression for a measured k_∞' in a mis-matched cell includes the following expressions:

$$k_\infty' = k^* - \frac{(1+TB^2)(1+L^2B^2)(1-p)L^2B^2}{1+(1-p)L^2B^2}$$

$$- \left[\frac{\tau B^2(1+L^2B^2)}{1+TB^2-n_1f_1(1-p)} \left(\frac{\Delta\phi}{\phi} + \frac{\Delta\phi^+}{\phi^+}\right)\right] \qquad (23)$$

$$+ \left[\frac{(1+L^2B^2)(1-n_1f_1(1+p)\Delta\phi x\Delta\phi^+}{1+TB^2-n_1f_1(1-)\qquad \phi x\ \phi^+}\right]$$

where now the reactor measurements are made in the mis-matched spectrum. This is especially applicable to this study in which the reactor loading consisted of four center cells (of varying enrichments as was learned later) surrounded by buffer cells of random particle

sizes and with an enrichment concentration different in all cases except the solid solution rods.

3. Determination of Measured k_∞' In The Fundamental Mode

The corrections to the measured quantities k_∞^* which are necessary to determine the k_∞' similar to what is calculated using the fundamental mode are listed in Table XVI.

The measured k_∞' derived from the experimental determination of k_∞^* are also listed in Table XVI. This table includes all the corrections necessary for the mis-match between cells and for the quantities necessary because k_∞^* and k_∞ are defined differently.

For the sake of convenience, the k_∞' in Table XVII has been corrected to a common enrichment; namely, 2 wt% PuO_2). These corrections were calculated by the two group model using the GRANIT and EGGNIT Codes to derive the necessary parameters as will be explained in the following section.

4. Theoretical Quantities of k_∞' for Water and Graphite Lattices

The parameters in equation (23) were calculated for the particle rods in a graphite lattice with 4-inch pitch and in a water moderated lattice with 1-inch pitch. The

Table XVI. List of Corrections to Determine k_∞' For Comparison To The Fundamental Model Calculation

Rod Type	8BMB	8SC	8BME	8P50	8B100	8P100	8B200	8P200	8B350
Particle Sizes	(Solid Solution)			50	110	110	200	200	330
Enrichment wt% PuO_2	1.98	2.08	2.10	2.29	2.48	2.47	2.35	2.41	2.42
k_∞^* (Null Reactivity Method)	1.544	1.544	NA	NA	NA	NA	NA	NA	NA
k^* (Unpoison technique)	1.549	1.547	1.545	1.541	1.547	1.538	1.547	1.538	1.551
Average	1.546	1.546	1.545	1.541	1.547	1.538	1.547	1.538	1.551
Correction $\frac{-(HTB^2)(1+L^2B^2)(1-p)(L^2B^2)}{1+(1-p)L^2B^2}$	0.047	-0.047	-0.047	-0.047	-0.047	-0.047	-0.046	-0.046	-0.046
Correction $\frac{-TB(1+L^2B^2)}{(1+TB^2-n_1f_1(1-p)}\left[\frac{\Delta\phi}{\phi}-\frac{\Delta\phi^+}{\phi^+}\right]$	0	0	+0.007	+0.017	+0.011	+0.015	+0.002	+0.008	-0.005
Correction $\frac{(1+L^2B^2)(1-n_1f_1)(1-p)}{1+TB^2-n_1f_1(1-p)}\left[\frac{\Delta\phi}{\phi}\times\frac{\Delta\phi^+}{\phi^+}\right]$	0	0	0	0	0	0	0	0	0
k_∞'	1.499	1.499	1.505	1.504	1.511	1.506	1.503	1.500	1.500
Corrections for Enrichment Differences	+0.002	-0.002	-0.010	-0.018	-0.021	-0.024	-0.019	-0.022	-0.022
k_∞' at 2 wt% PuO_2	+1.501	+1.497	1.495	1.493	1.490	1.482	1.484	1.478	1.478
	+0.010	+0.010	±0.010	±0.010	±0.010	±0.010	±0.010	±0.010	±0.010
Calculated k_∞'	1.500	1.500	1.500	1.496	1.492	1.492	1.484	1.484	1.474

Table XVII. Calculated k_∞ For Graphite And Water Moderated Lattice With Respect To Particle Size

(Mixed Oxide Rods 2 wt% PuO_2-UO_2)

Graphite Lattice (4" pitch)

Particle Size (microns)	$n_1 f_1$	$(\nu\Sigma f)_2$	Σ_{a2}	p	k_∞
SS	0.53781	6.96193-3	4.12665-3	0.83713	1.500 ±.001
50	0.53860	6.81798-3	4.05603-3	0.83810	1.496 ±.005
100	0.53906	6.67881-3	3.98784-3	0.83916	1.492 ±.005
200	0.54089	6.41329-3	3.85767-3	0.84123	1.484 ±.005
350	0.54340	6.04109-3	3.68050-3	0.84340	1.474 ±.005

Water Lattice (1" pitch)

SS	0.66298	1.20249-1	8.07289-2	0.83838	1.356 ±.001
50	0.66482	1.17606-1	7.94142-2	0.83950	1.350 ±.003
100	0.66679	1.14905-1	7.79200-2	0.84068	1.346 ±.003
200	0.67000	1.10200-1	7.47291-2	0.84257	1.331 ±.003
350	0.67504	1.03598-1	7.24500-2	0.84545	1.313 ±.003

thermal spectrum parameters denoted by the subscript (2) were derived in GRANIT calculations and the epi-thermal (>.683 ev) spectral quantities were derived using the EGGNIT-GRAINS code.

The statistical uncertainty in the calculated k_∞ is considered to be approximately one-half of the uncertainty in the measured k_∞ for the following reasons.

The 5 mk error for the calculations is based on the errors in the determination of the particle size and the enrichment. The particle sizes are only certain to ±40 microns and the enrichment ±0.1 percent (absolute). It was possible to estimate the variations in the calculated multiplication factor due to these two unknowns.

H. Conclusions Concerning Particle Effects From This Study

The experimental and theoretical parameters from this experiment have been summarized in Table XVIII for the convenience of the reader. The conclusions drawn from this experimental and theoretical analysis are as follows:

- The null reactivity technique and adjoint weighted cross section technique can measure similar quantities provided the changes in the center cell do not cause a high degree of flux mis-match during the null reactivity measurements.

Table XVIII. Summary of Experimental and Theoretical Parameters of Particle Fuel

Parameters	Rod Designator									
	8SC	8BMB	8BME	8P50	8B100	8P100	8B200	8P200	8B350	8RA350
Particle Size (microns)	(Solid Solution)			50	110	110	200	200	330	330
Enrichment (wt% PuO_2)	2.08	1.98	2.10	2.29	2.48	2.47	2.35	2.41	2.42	2.47
Measured Relative Absorption of Plutonium (thermal)	1.0	1.0	1.0	-	-	-	-	-	0.820	0.820
Calculated Relative Absorption of Plutonium (thermal)	1.0	1.0	1.0	0.968	0.930	0.930	0.878	0.878	0.815	0.815
Calculated k_∞' at 2 wt% Enrichment		1.500 .005		1.496 .005	1.492 .005		1.484 .005		1.474	
Measured k_∞' Corrected to 2 wt% Enrichment (Unpoisoned Technique)	1.497 ±.010	1.501 ±.010	1.495 ±.013	1.493 ±.010	1.490 ±.010	1.482 ±.010	1.484 ±.010	1.478 ±.010	1.478 ±.010	1.478 ±.012
Measured k_∞' Corrected to 2 wt% Enrichment (Poisoned Technique)	1.499 ±.010	1.496 ±.010	1.486 ±.015							

- The reactivity trends with respect to particle size are apparent from the measurements even though absolute effects are somewhat masked by the statistical uncertainty in the measurements.
- The measured relative absorption rates in the plutonium and uranium with respect to particle size which are derived from the foil data are in excellent agreement with the calculated quantities derived by the GRANIT code.
- The measured enrichment in the fuel rods by the gamma scanning technique explains the discrepancies in the reactivity worth of the rods with respect to particle size.
- In general, the experiment has been a verification of the particle theory and demonstrates the need for strong quality control in the manufacture and use of mixed oxide fuel.
- For power reactor fuels, the particle size is not important to economics and fuel lifetime unless it exceeds 200 microns. Above this size the potential reactivity will decrease sufficiently to affect the efficiency of the reactor system.

REFERENCES

1. R. K. Lane, L. W. Nordheim and J. B. Sampson, "Resonance Absorption in Materials with GRAIN Structure," Nucl. Sci. Eng., 14, No. 4, 390-396 (1963).

2. R. A. Lewis and T. J. Connally, "Resonance Absorption in Particles," Nucl. Sci. Eng., 24, No. 1, January 1966.

3. M. A. Robkin, Final Report on Pu Recycle for H_2O Moderated Reactors, GEAP-4907, August 1965.

4. D. J. Donahue, D. D. Lanning, R. A. Bennett and R. E. Heineman, "Determination of k_∞ from Critical Experiments in the PCTR," Nucl. Sci. Eng., Vol. 4, pp.297 (1958).

5. R. E. Heineman, "On The Interpretation of Reactivity Measurements of Reactor Media," TRANS. ANS, Vol. 8, No. 2, pp.532, 1965.

6. E. P. Lippincott, C. R. Richey and D. D. Lanning, "Definition of the Infinite Neutron Multiplication Factors Measured by the PCTR Poisoned and Unpoisoned Technique," Reactor Physics Quarterly Report, July, August, September, 1969, Battelle Memorial Institute, Pacific Northwest Laboratories, Richland, Washington

7. H. R. Wisely, "Feasibility Study of PuO_2 (Poisoned Particle) Preparation," letter to F. G. Dawson, October 27, 1965.

8. D. E. Blahnik, "Irradiation Plasma Progress Report," Unpublished manuscript.

9. R. A. Bennett, "Effective Resonance Integrals of Copper and Gold," Nuclear Physics Research Quarterly Report, October, November, December, 1959, HW-63576, General Electric Company, Hanford Laboratories, Richland, Washington, January 1960.

10. G. E. Hansen and N. A. Hill, "A Thermal Column Study in the PCTR," Reactor Physics Department Technical Activities Quarterly Report July, August, September, 1966, Battelle Memorial Institute, Pacific Northwest Laboratories, Richland, Washington, October, 1966.

11. J. R. Lilley, APDAC-I, A PCTR Data Analysis Code for the IBM-709, HW-63592, September 17, 1970.

12. Letter from W. Y. Matsumoto to A. D. Vaughan, "Results from Analysis of Plutonium Aluminum Foil," March 26, 1970.

13. F. R. Mynatt, Users Manual for DOT, K-1694, Oak Ridge Gaseous Diffusion Plant, Oak Ridge, Tennessee (Unpublished).

14. H. C. Honeck, THERMOS, A Thermalized Transport Theory Code for Reactor Lattice Calculations, BNL-5826, Brookhaven National Laboratory, Upton, NY, September, 1969.

15. C. L. Bennett, "GRANIT: A Code for Calculating Position Dependent Thermal Neutron Spectra in Doubly Heterogeneous Systems by the Integral Transport Method", Technical Activities Quarterly Report AEC Reactor Development and Technology Programs July, August, September 1970, BNWL-1522-1, Battelle Memorial Institute, Pacific Northwest Laboratories, Richland, Washington, October, 1970.

16. C. R. Richey, EGGNIT: A Multigroup Cross Section Code BNWL-1203, Battelle Memorial Institute, Pacific Northwest Laboratories, Richland, Washington, November, 1969.

17. R. K. Lane, L. W. Nordheim and J. B. Sampson, "Resonance Absorption in Materials with GRAIN Structure," Nucl. Sci. Eng., 14, No. 4, 390-396 (1963).

18. A. D. Vaughn, "Comparison of Calculated Versus Measured Relative Reaction Rates with Respect to Particle Size in UO_2-PuO_2 Fuel Rod Specimens," Reactor Physics Quarterly Report October, November, December 1969, BNWL-1304, Battelle Memorial Institute, Pacific Northwest Laboratories, Richland, Washington, February, 1970.

19. Letter from W. Y. Matsumoto to A. d. Vaughn, "Results from Analysis of UO_2-PuO_2 Fuel Rod Specimens," March 25, 1970.

20. Lederer, Hollander, Perlman, Table of Isotopes, 6th Edition. John Wiley & Sons, New York, 1967.

21. J. Peter, H. Schumacker, The Gamma Spectrometer Determination of 241-Pu/239-Pu Ratio and its Application to Fuel Burnup, EIR-172, January, 1970.

22. Gladys White Grodstein, X-Ray Attenuation Coefficients from 10 keV to 100 MeV, NBS Circular 583, April 30, 1957. U. S. Government Printing Office.

23. Theodore Rockwell III, ed., Reactor Shielding Design Manual, First Edition, pp. 370, D. Van Nostrand Co. (1956).

24. K. B. Stewart, BNW Master Library, BNWL-CC-325, Battelle Memorial Institute, Pacific Northwest Laboratories, Richland, Washington, (1965).

25. A. M. Weinberg and E. P. Wigner, The Physical Theory of Neutron Chain Reactors, The University of Chicago Press, 1958.

26. L. W. Nordheim, The Theory of Resonance Absorption, GA-638 (Rev.), General Atomic Corporation, San Diego, California (1959).

27. Joan Bell, SUMIT - An IBM 7090 Program for the Compilation of Crystalline Scattering Kernels, GA-2492, General Atomic Corporation, San Diego, California (1962).

28. G. W. Dixon and R. Sher, "Measurements of Thermal Neutron Spectra in Heterogeneous Lattices by Foil Activation," Nucl. Sci. Eng., Vol. 41, pp.357-366 (1970).

29. Ward W. Engle, Jr., "A Users Manual for ANISN, A One Dimensional Discrete Ordinates Transport Code With An Isotopic Scattering," K-1693, March 30, 1967.

30. E. P. Lippincott, Derivation of Corrections to k_∞ in the Two Group Approximation, BNWL-1560, Battelle Memorial Institute, Pacific Northwest Laboratories, Richland, Washington, May, 1970.

APPENDIX A

Nitrogen Correction

Determination of the reactivity worth of the nitrogen ($\Delta\rho_N$) which fills the cavity formed by the removal of the central supercell is inferred from a copper sensitivity, S_{cm}^{cavity}, measurement using the expression:

$$\Delta\rho_N = DC \frac{P}{T} (M_N)(1-C) S_{cu}^{cavity} \qquad (24)$$

where, D = thermal disadvantage factor for the thickness of the copper (.010-in.) used in the determination of S

$$S_{cu}^{cavity} = 1.0110$$

$$S_{cu}^{cavity} = \frac{\Delta\rho_{cu}^{cavity}}{M_{cu}^{cavity}}, \text{ ¢/gram of copper}$$

$\Delta\rho_{cu}^{cavity}$ = reactivity worth of mass of copper, M_{cu}^{cavity}, in the cell cavity, ¢.

P = atmospheric pressure during reactivity measurement, mb.

T = ambient temperature in cavity during reactivity measurement, °K;

M_N = mass of nitrogen (at standard temperature and pressure) in the cavity

$$C = \frac{\sigma_o^N}{\sigma_o^{cu}} \frac{A^{cu}}{A^N} \frac{T_o}{P_o} \qquad (25)$$

where σ_o^N = 2200 m/sec microscopic absorption cross section of nitrogen - 1.88 b.

σ_o^{Cu} = 2200 m/sec microscopic absorption cross section of natural copper = 3.79 b

A^{cu}, A^N = copper and nitrogen atomic weights

T_o, P_o = standard temperature and pressure

The nitrogen effect for the four center cells was approximately 0.9¢ reactivity or equivalent to 9.0 grams of copper for four cells and approximately 2.0 mk in the k_∞ measurement.

APPENDIX B

Manufacturing Processes of Particle Fuel

The manufacturing process to convert the basic fuel material into pellet form was developed through several changes by successive metallurgical engineers so that three different sets of particle fuel rods were available for the experiment. The various rod types are distinguished by the name of the fuel design engineer who developed the particle shaping process, and the size of the particle in each rod.

1. Plutonium Particle Fabrication by H. R. Wiseley
   - Starting material was Calciner-Oxide, low fired from the oxalate of 350 to 400°C. This gives an extremely fine initial particle size.
   - The PuO_2 was mixed with a poly-vinyl alcohol binder and pre-pressed into discs, 1/16 inch thick and 2-inches in diameter. This was done to give a uniform green density to all the PuO_2 particles of about 50% T.D.
   - The discs broken through a screen to obtain 1/16 inch cubes. These cubes were jet milled to make spheres. Given sized spheres are chosen by double screen systems.

- The PuO_2 spheres were fired at a temperature of approximately 1650°C to get particles of approximately 80% T.D. These particles were again size selected by the double screen system.

2. Mixed Oxide Fuel Element Fabrication

- The sintered spheres of PuO_2 of a given size were blended with arc fused UO_2 in the following particle size ratios.

Mesh Size		Percent of UO_2
- 65 to + 100	=	50%
-100 to + 200	=	30%
-325	=	20%

- Moisture was added to the blend (water) to make the blend hold together. The blend was pushed through a 12 or 14 mesh screen to form lumps which were rounded and then slightly dried.
- The rounded lumps were loaded into a die and pressed into a pellet with a pressure of 40 tons/in^2. This formed a fuel pellet of 80 to 80% T.D.
- The pellets were dried in a dryer and then loaded into the tubes to form a finished mixed oxide fuel element.

3. Particle Shaping Process of Dr. Robert Anicetti

A second set of particle type fuel rods were constructed using a process developed by Dr. Robert Anicetti. This new process is similar to the process of H. R. Wiseley, however, a dynapacking method was used to obtain the PuO_2 pellets in place of the cold pressing method. Therefore, these new rods were made by a dynapacking and jet milling process. The process did not increase the density of the pellets which remained at ~80%.

4. Particle Shaping Process of D. E. Blahnik

An improved particle shaping process was developed by D. E. Blahnik using the RF induction plasma process starting in June 1967. Prior to this time all the spheroids were made by using the jet milling process. The equipment includes water cooled plasma tubes, an oxygen system for increasing the fuel gas enthalpy, and an infrared furnace for preparing the PuO_2 up to 1000°C. A process flow chart of this system is presented in Figure 1.

The RF induction plasma process resulted in the manufacture of dense, high purity spheres which are essentially free from smearable contamination. The

Figure 1. PCTR Fuel Rod Fabrication Flow Sheet

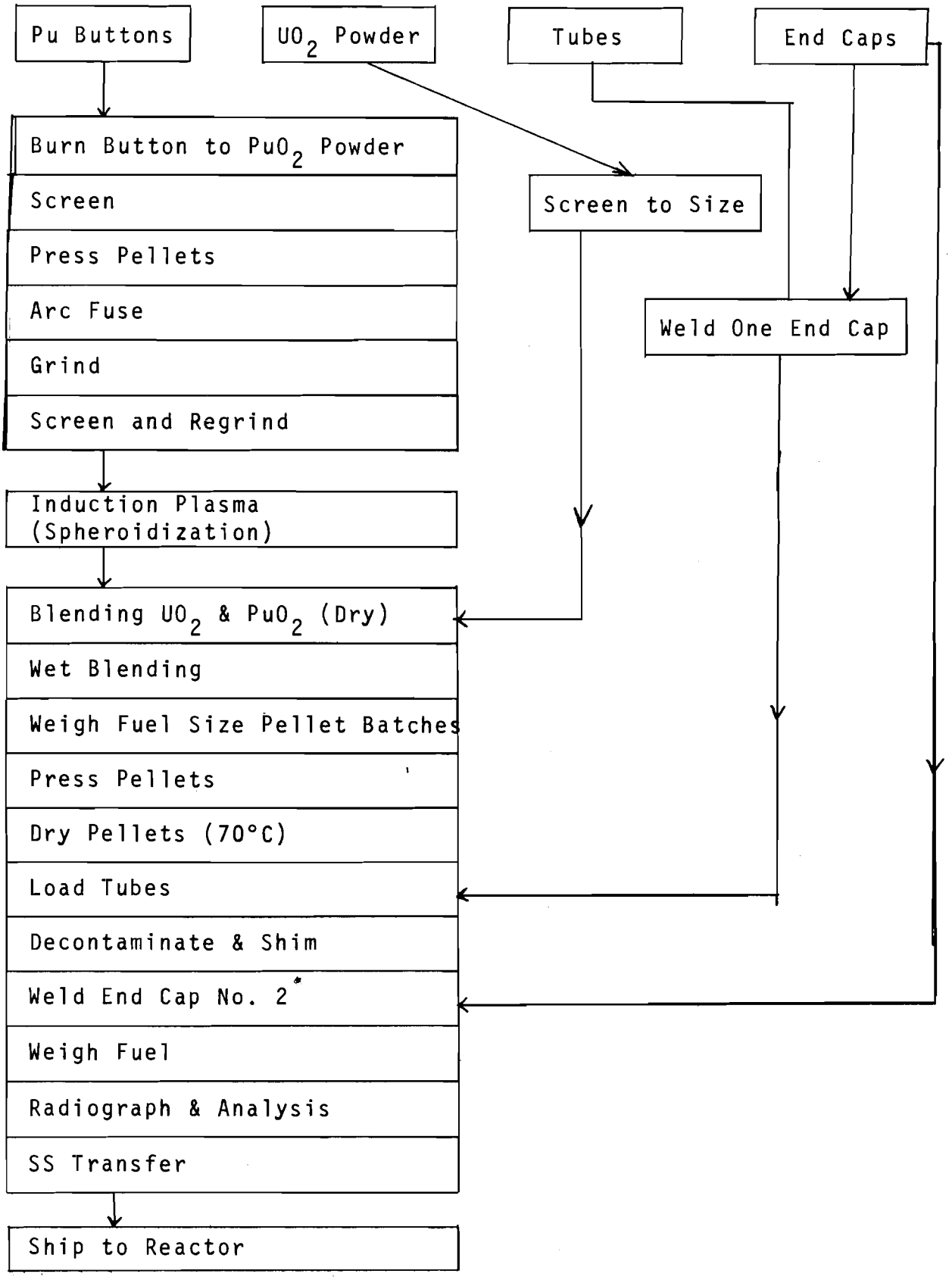

spectro chemical analysis prior to PuO_2 speroidization and afterwards indicates how the material was purified (apparently vaporized while passing through the plasma) (see Table I). The spheres are thermally and chemically stable.

Table I. Purity Samples Before and After Plasma Process[8]

Element	Parts per Million	
	Before Plasma Process	After Plasma Process
Ag	< .1	< .1
Al	100	-
B	< .1	-
Be	.5	-
Cb	< 1	-
Cr	< 5	-
Cu	200	100
Mg	50	< 5
Mu	10	5
Na	< 1	< 2
Ni	2	10
P	100	-
Pb	2	-
Si	115	< 5
Sn	< .5	< 5
Zn	< 50	-

APPENDIX C

The Theoretical Model Used for k_∞^*

Identification of k_∞ with k_{eff}

The following development is based on the definition of the effective neutron multiplication factor (k_{eff}) as the total neutron production divided by the sum of the total neutron loss due to absorption and leakage. The values of k_∞ calculated from these experiments are consistent with this definition of k_{eff}.

Let us cast the analysis in a two-energy group formulation recognizing that multigraoup calculations are appropriate and should yield valid comparisons with these experiments when the multigroup results are interpreted properly.

The neutron balance equations for the two-energy groups can be written as

$$D_1\nabla^2\phi_1 - \Sigma_1\phi\phi_1 - \Sigma_{1\to2}\phi_1 + (\nu\Sigma_f)_1\phi_1 + (\nu\Sigma_f)_2\phi_2 = 0 \qquad (26)$$

and

$$D_2\nabla^2\phi_2 - \Sigma_2\phi_2 + \Sigma_{1\to2}\phi_1 = 0 \qquad (27)$$

The notation can be simplified if we rewrite these two equation as

$$-L_1 - A_1 - P_{21} + P_{11} + P_{12} = 0 \tag{28}$$

and

$$-L_2 - A_2 +)_{21} = 0 \tag{29}$$

The symbols A_i and L_i refer to absorption and leakage respectively in the energy group i. The symbol P_{ij} refers to the production of neutrons in energy group i due to reactions in energy group j.

The total production of neutrons (TP) and the total loss of neutrons due to absorption (TA) and leakage (TL) can be written as follows:

$$TP = P_{11} + P_{12} \tag{30}$$

$$TA = A_1 + A_2 \tag{31}$$

$$TL = L_1 + L_2 \tag{32}$$

Simultaneous solution of equations (28) and (29) for the total production of neutrons gives

$$TP = P_{11} + P_{12} = A_1 + A_2 + L_1 + L_2 \tag{33}$$

The standard form[4] of the equations relating k_{eff} and k_∞ in two group theory can be written as:

$k_{eff} = k_\infty$ (non leakage probability from group 1)

(non leakage probability from group 2)

or

$$k_{eff} = k_{\infty} \frac{1}{1 + \frac{L_1}{A_1} + P_{21}} \frac{1}{1 + \frac{L_2}{A_2}} \tag{34}$$

The two group equation for k becomes

$$k_{\infty} = \frac{A_1 + A_2 + L_1 + L_2}{A_2} \frac{P_{21}}{A_1 + P_{21}} \tag{35}$$

A small amount of algebra using equations (33), (34) and (35) leads to the original definition of k_{eff}.

$$k_{eff} = \frac{TP}{TA + TL} \tag{36}$$

The Evaluation of the Experimental k_{∞}^*

The PCTR method determines the k_{∞}^* of an infinite unpoisoned lattice by poisoning the lattice so that the infinite medium neutron multiplication factor of the poisoned lattice, k_{∞}, is unity. In the following development, the unprimed symbols refer to quantities in the unpoisoned lattice and the primed symbols refer to the corresponding quantities in the poisoned lattice.

Equation (35) can be used to write expressions for the infinite neutron multiplication factor for the respective poisoned and unpoisoned lattice

$$\text{Unpoisoned } k_{\infty}^* = \frac{A_1 + A_2 + L_1 + L_2}{A_2} \frac{P_{21}}{A_1 + P_{21}} \tag{37}$$

$$\text{Poisoned } k_\infty' = 1 = \frac{A_1' + A_2' + L_1' + L_2' + A_{2a}' + A_{1a}'}{A_2' + A_{2a}'} \qquad (38)$$

$$\frac{P_{21}'}{A_1' + A_{1a}' + P_{21}'}$$

The symbols A_{2a}' and A_{1a}' are the respective subcadmium and epicadmium absorptions in the poison.

If we define neutron escape probabilities in the unpoisoned and poisoned lattice, respectively, as

$$p = \frac{P_{21}}{P_{21} + A_1} \quad \text{and} \quad p' = \frac{P_{21}'}{P_{21}' + A_1'}$$

and make use of equation (33), equations (37) and (38) become

$$k_\infty^* - \frac{TP}{A_2} p \qquad (39)$$

and

$$k = 1 = \frac{TP}{A_2 + A_{2a}} p \; \frac{1}{1 + \frac{A_{1a}}{A_1} + P_{21}} \qquad (40)$$

The unpoisoned k_∞^* can be rewritten as equation (39) divided by equation (40)

$$k_\infty^* = \frac{TP}{A_2} \frac{A_2' + A_{2a}'}{TP'} \frac{p}{p'}(1 + \frac{A_{1a}'}{A_1'} + P_{21}' \qquad (41)$$

Equation (41) is almost the expression used to calculate k_∞ from the experimental data. Some algebra is required in obtaining the final result as well as observing that the

addition of the poison does not change the excape probability (i.e., $p = p'$)

After the escape probabilities are canceled, equation (41) can be rewritten as

$$k_{\infty}^{*} = \frac{TP}{TP'} \frac{A_2' + A_{2a}'}{A_2} + \frac{(A_2' + A_{2a}')}{A_1' + P_{21}'} \frac{A_{1a}}{A_2} \tag{42}$$

In an infinite system

$$P_{21}' = A_2' + A_{2a}' \tag{43}$$

and

$$\frac{A_2' + A_{2a}'}{A_1' + P_{21}'} = p = p' \tag{44}$$

The expression used to evaluate the experimental k values is obtained by substituting (43) into (44). The result is

$$k_{\infty}^{*} = \frac{TP}{A_2} \frac{A_2' + A_{2a}' + p A_{1a}'}{TP'} \tag{45}$$

BNWL-1608

Special Distribution
in Category UC-80

DISTRIBUTION

No. of Copies

OFFSITE

1 AEC Chicago Patent Group

G. H. Lee

7 AEC Division of Reactor Development and Technology

Director, RDT
Asst Dir., Project Management
Chief, Water Projects Branch (2)
Asst Dir., Reactor Technology
Chief, Reactor Physics Branch (2)

3 AEC Division of Reactor Licensing

Director, DRL

2 AEC Division of Reactor Standards

Director, DRS

3 AEC Division of Technical Information Extension

1 Argonne National Laboratory (AEC)

R. Avery

1 Babcock and Wilcox
P. O. Box 1260
Lynchburg, Va. 24505

H. M. Jones

1 Bhabha Atomic Research Centre
Theoretical Physics Section/RED
Central Complex Bldg.
Trombay, Bombay-85, India

S. R. Dwivedi

1 Brookhaven National Laboratory

H. J. C. Kouts

No. of Copies

1 Tennessee Valley Authority
503 Power Bldg.
6th & Market
Chattanooga, Tennessee 27402

R. H. Davidson

1 Combustion Engineering
P. O. Box 500
Windsor, Connecticut 06095

S. Visner

1 CNEN - Centro Studi-Nucleaire
Casaccia, Rome, Italy

Ugo Farinelli

3 Edison Electric Institute
750 Third Avenue
New York, N. Y. 10017

John J. Kearney (2)
George Watkins

2 E. I. du Pont deNemours & Co., Inc., SRL

G. Dessauer
H. Honeck

1 ENEL
Via G. B. Martini
(Pizaaz Verdi)
Rome, Italy

Mr. Paoletti Gualandi

7 General Electric Co., San Jose
175 Curtner Avenue
San Jose, California 95112

R. L. Crowther
D. L. Fischer
A. D. Vaughn (5)

No. of Copies

1 General Electric Co., Vallecitos Atomic Lab.
P. O. Box 846
Pleasanton, California

T. M. Snyder

2 Gulf General Atomic Co.
P. O. Box 608
San Diego, California 92112

R. C. Dahlberg
H. B. Stewart

1 Japan Atomic Energy Institute
Tokaimura, Ibarakiken, Japan

Shojiro Matsurra, JPDR-TCA

1 Kerr-McGee Corp.
133 NW Robert S. Kerr Ave.
Oklahoma City, Oklahoma 73102

Parker Dunn

1 Nuclear Fuels Services, Inc.
Suite 600
6000 Executive Blvd.
Rockville, Maryland 20852

J. D. McDaniels

1 Nuclear Materials and Equipment Corp.
Penn Center
Apollo, Penn. 15613

K. Puechl

1 NUKEM
D-645, NANAU
POSTFACH 869
Germany

Mr. Wolgang K. L. Jager

No. of Copies

1 Pakistan Institute of Nuclear Sci. & Tech.
P. O. Nilore
Rawalpindi, Pakistan

M. A. Mannan

1 Philadelphia Electric Company
1000 Chestnut Street
Philadelphia 5, Pa.

Mr. Wayne C. Astley

1 Power Reactor & Nuclear Fuel Development Corp.
9-13, 1- chome, Akasaka,
Minato-ku, Tokyo, Japan

Setsuo Kobayashi

1 S. C. K. - C. E. N.
MOL-DONK
Belgium

Dr. H. Vanden Broeck
BRL.

1 United Nuclear Corporation
Research & Engineering Center
Grasslands Road
Elmsford, New York 10523

J. R. Tomonto

4 Westinghouse Electric Corporation
Atomic Power Division
P. O. Box 355
Pittsburg, Penn 15230

C. L. Bennett
R. J. French
W. L. Orr
J. R. Worden

No. of
Copies

ONSITE - HANFORD

1 AEC Chicago Patent Group

R. M. Poteat

5 RDT Assistant Director for Northwest Programs

W. E. Fry
P. G. Holsted
H. A. House
J. B. Kitchen
T. A. Nemzek

1 AEC Richland Operations Office

M. R. Schneller

48 Battelle-Northwest

J. M. Batch
C. A. Bennett
S. H. Bush
J. L. Carter
N. E. Carter
D. E. Christensen
F. G. Dawson
D. E. Geonigi
L. J. Federico
J. W. Finnigan
J. C. Fox
M. D. Freshley
S. Goldsmith
H. L. Henry
U. P. Jenquin
D. A. Kottwitz
D. C. Lehfeldt
B. R. Leonard
R. C. Liikala
C. W. Lindenmeier
E. P. Lippincott
D. F. Newman
D. R. Oden
R. S. Paul
D. L. Prezbindowski
W. L. Purcell
W. D. Richmond
L. C. Schmid (5)
G. D. Seybold
R. I. Smith
D. H. Thomsen
V. O. Uotinen
L. D. Williams
N. G. Wittenbrock
W. C. Wolkenhauer
M. G. Zimmerman
BNWL Legal (2)
Technical Information (5)
Technical Publications